

A Distribution-Free Description of Fragmentation by Blasting Based on Dimensional Analysis

José A. Sanchidrián¹  · Finn Ouchterlony²

Received: 14 April 2016 / Accepted: 9 November 2016 / Published online: 28 November 2016
© The Author(s) 2016. This article is published with open access at Springerlink.com

Abstract A model for fragmentation in bench blasting is developed from dimensional analysis adapted from asteroid collision theory, to which two factors have been added: one describing the discontinuities spacing and orientation and another the delay between successive contiguous shots. The formulae are calibrated by nonlinear fits to 169 bench blasts in different sites and rock types, bench geometries and delay times, for which the blast design data and the size distributions of the muckpile obtained by sieving were available. Percentile sizes of the fragments distribution are obtained as the product of a rock mass structural factor, a rock strength-to-explosive energy ratio, a bench shape factor, a scale factor or characteristic size and a function of the in-row delay. The rock structure is described by means of the joints' mean spacing and orientation with respect to the free face. The strength property chosen is the strain energy at rupture that, together with the explosive energy density, forms a combined rock strength/explosive energy factor. The model is applicable from 5 to 100 percentile sizes, with all parameters determined from the fits significant to a 0.05 level. The expected error of the prediction is below 25% at any percentile. These errors are half to one-third of the errors expected with the best prediction models available to date.

Keywords Rock blasting · Fragmentation prediction · Size distribution · Dimensional analysis · Kuz-Ram · Swebrec

✉ José A. Sanchidrián
ja.sanchidrian@upm.es

¹ ETSI Minas y Energía, Universidad Politécnica de Madrid, Madrid, Spain

² Department of Mineral Resources Engineering, Montanuniversitaet Leoben, Leoben, Austria

1 Introduction

The main goal of rock blasting is the fragmentation of the rock mass. Prediction of the size distribution of the fragmented rock from the rock mass characteristics, the blast design parameters (both in terms of the geometry and of the initiation sequence) and the explosive properties is a challenge that has been undertaken for decades, and is currently available to the blasting engineer in the form of formulae that relate the parameters of a given size distribution function to the rock properties and the blast design parameters.

One of the most relevant fragmentation by blasting formulae is the Kuznetsov (1973) one:

$$x_m = Aq^{-0.8}Q^{1/6} \quad (1)$$

where x_m is the mean fragment size in cm, A is a rock strength factor in the range 7–13, q is the powder factor (or specific charge, or charge concentration—explosive mass per unit rock volume) in kg/m^3 and Q is the charge per hole in kg. These three factors comply essentially with the expected behavior of rock fragmentation by blasting. Essentially, the Kuznetsov formula means that (1) the harder the rock, the bigger the fragments; (2) the higher the specific amount (powder factor) of explosive, the smaller the fragments; and (3) the larger the scale (the charge per hole is used as scale factor, and larger charges per hole indicate larger drill patterns), the larger the fragments. In Eq. 1, the amounts of explosive in the powder factor and the charge per hole are given in TNT equivalent mass. Such equivalent mass can be calculated multiplying the mass of explosive by its relative strength with respect to TNT; if such strength is θ , Eq. 1 can be written as (Kuznetsov 1973, Eq. 12):

Table 1 Blast and fragmentation data: blast sites, rock types and references

Blast site	Rock	References
El Alto quarry, Spain	Limestone	Segarra and Sanchidrián (2003), Sanchidrián et al. (2006)
Mt. Coot-tha quarry, Australia	Hornfels	Kojovic et al. (1995), LeJuge and Cox (1995)
Bårarp quarry, Sweden	Granitic gneiss	Olsson and Bergqvist (2002), Moser et al. (2003)
Kållerød quarry, Sweden	Gneissic granite	Gynnemo (1997)
Billingsryd quarry, Sweden	Dolerite	Gynnemo (1997)
Rolla quarry, MO, USA	Dolomite	Otterness et al. (1991)
High Forest quarry, MN, USA	Dolomitic limestone	Ash (1973), Dick et al. (1973)
Guan Shan copper mine, Jiang Shu, China	Rhyoporphyry	Ma et al. (1983)
Rolla quarry, MO, USA	Dolomite	Stagg and Nutting (1987)
Waterloo quarry, IA, USA	Limestone	Stagg et al. (1989)
St Paul Park quarry, MN, USA	Dolomite	Stagg and Rholl (1987)
Granite Falls quarry, MN, USA	Granitic gneiss	Stagg and Otterness (1995)
Manitowoc quarry, WI, USA	Dolomite	Stagg and Otterness (1995)
Vändle quarry, Sweden	Granite	Ouchterlony et al. (2005, 2006), Ouchterlony and Moser (2006), Liu et al. (2011)
Långåsen quarry, Sweden	Granodiorite	Ouchterlony et al. (2010, 2015)
Rolla quarry, MO, USA	Dolomite	Smith (1976)
Rolla quarry, MO, USA	Dolomite	Brinkmann (1982)
Rolla quarry, MO, USA	Dolomite	Bleakney (1984)

$$x_m = Aq^{-0.8}Q^{1/6}\theta^{-19/30} \quad (2)$$

in which q and Q refer to actual mass of explosive of relative strength θ . Equation 1 or its equivalent Eq. 2 is written originally for the mean size x_m of a Rosin–Rammler (RR) distribution (Rosin and Rammler 1933; Weibull 1939, 1951) that was assumed to accurately describe the fragmented rock. The Rosin–Rammler, or Weibull, cumulative distribution function is:

$$P(x) = 1 - \exp\left[-\left(\frac{x}{x_c}\right)^n\right] = 1 - \exp\left[-\ln 2\left(\frac{x}{x_{50}}\right)^n\right] \quad (3)$$

where x_c is the characteristic size (the size for which the passing fraction is $1 - 1/e$, or 63.2%) and n is a shape factor, usually quoted as uniformity index; the expression on the right is written with the median size x_{50} instead of x_c . The use of the RR distribution for rock fragmented by blasting had been positively assessed by Baron and Sirtuyuk (1967) and Koshelev et al. (1971), which is used by Kuznetsov (1973).

The Soviet literature of the time does not make it entirely clear whether Eqs. 1 or 2 refer to the mean or the characteristic size (which value is close to the mean if the shape index of the distribution is not much different than one). There has been some controversy (Spathis

2004, 2009, 2012, 2016; Ouchterlony 2016a, b) about the actual size that the Kuznetsov formula was addressing. For all practical purposes, it has been calibrated, tailored and used over the years to estimate the median size x_{50} (Cunningham 1987, 2005; Rollins and Wang 1990; Raina et al. 2002, 2009; Liu 2006; Cáceres Saavedra et al. 2006; Borquez 2006; Rodger and Gricius 2006; Vanbrabant and Espinosa Escobar 2006; Mitrovic et al. 2009; Engin 2009; Gheibie et al. 2009a, b; Bekkers 2009; McKenzie 2012; Sellers et al. 2012; Faramarzi et al. 2015; Jahani and Taji 2015; Singh et al. 2015; Adebola et al. 2016).

Kuznetsov derived his formula based on blasting tests in limestone specimens reported by Koshelev et al. (1971). These consisted of eleven small- to mid-scale shots in irregular limestone blocks, with RDX charges of 0.5–500 g. Kuznetsov then assessed the formula with some data from large-scale tests by Marchenko (1965), 6 blasts in limestone, 6 blasts in a medium-hard rock and 14 blasts in hard and very hard rock (the exact rock type is not reported, nor is the explosive used). A values recommended by Kuznetsov were 7, 10 and 13 for medium-to-hard, hard fissured and hard massive rocks, respectively. Kuznetsov mentions that the mean deviation of experimental data from the theoretical (i.e., predicted) data is $\pm 15\%$; a detailed analysis of the data and the predictions by Eqs. 1 or 2 gives a mean error of 9%, with minimum and

maximum errors of -42 and 55%, respectively (Ouchterlony 2016a). This matter will be re-assessed in this work.

About ten years after its publication, the Kuznetsov formula was popularized by Cunningham (1983), who wrote it so as to use the relative weight strength with respect to ANFO, the standard explosive in civil applications, instead of TNT, in what became the popular Kuz-Ram model. In his text, Cunningham uses the term ‘mean fragment size,’ but his mathematical definition of it implies the median; he in fact uses the symbol x_{50} . In the Kuz-Ram papers that followed (Cunningham 1987, 2005), the term mean is also used but again contradicted by figures and equations that imply x_{50} :

$$x_{50} = Aq^{-0.8} Q^{1/6} \left(\frac{RWS}{115} \right)^{-19/30} \tag{4}$$

Here RWS is the relative weight strength (heat of explosion, or energy in general, ratio with respect to ANFO, in percent; 115 is the relative weight strength of TNT). Cunningham (1987) adapted a blastability index proposed by Lilly (1986) to replace Kuznetsov’s numerical rock factor:

$$A = 0.06 \cdot (RMD + JF + RDI + HF) \tag{5}$$

The form of the rock mass description term (RMD) has had some changes over the years; in its final form (Cunningham 2005), it is:

RMD = 10 (powdery/friable), JF (if vertical joints) or 50 (massive);

JF (joint factor) = JPS (joint plane spacing) + JPA (joint plane angle);

JPS = 10 (average joint spacing $S_j < 0.1$ m), 20 ($0.1 \leq S_j < 0.3$ m), 80 ($0.3 \text{ m} \leq S_j < 0.95 \cdot (B \cdot S)^{1/2}$, B and S being burden and spacing), 50 ($S_j > (B \cdot S)^{1/2}$). Cunningham (2005) incorporates a joint condition correction factor that multiplies the joint plane spacing, with value 1, 1.5 and 2 for tight, relaxed and gouge-filled joints, respectively;

JPA = 20 (dip out of face), 30 (strike perpendicular to face) or 40 (dip into face). Cunningham does not give a JPA value for horizontal planes but Lilly (1986) assigns them JPA = 10.

The rock density influence (RDI) is:

$$RDI = 0.025 \cdot \rho - 50.$$

ρ being density (kg/m³). Finally, the hardness factor (HF) is:

$$\begin{aligned} HF &= E/3 \text{ if } E < 50, \text{ or} \\ HF &= \sigma_c/5 \text{ if } E > 50. \end{aligned}$$

σ_c and E being uniaxial compressive strength (MPa) and Young’s modulus (GPa).

The form of RMD implies that JF may enter twice in Eq. 5, directly and through RMD. The direct term in Eq. 5 Cunningham (1987) is in all probability a printing error and Cunningham (2005) removed it in later Kuz-Ram model updates, so that:

$$A = 0.06 \cdot (RMD + RDI + HF) \tag{6}$$

Cunningham (2005) also incorporated a delay-dependent factor in the central size formula, based on Bergmann et al. (1974) data:

$$\begin{aligned} A_r &= 0.66 \left(\frac{\Delta T}{T_{\max}} \right)^3 - 0.13 \left(\frac{\Delta T}{T_{\max}} \right)^2 - 1.58 \left(\frac{\Delta T}{T_{\max}} \right) + 2.1, \\ &\quad \times \frac{\Delta T}{T_{\max}} < 1 \\ A_r &= 0.9 + 0.1 \left(\frac{\Delta T}{T_{\max}} - 1 \right), \quad \frac{\Delta T}{T_{\max}} > 1 \end{aligned} \tag{7}$$

where $T_{\max} = 15.6B/c_P$; ΔT is in-row delay (ms), B is burden (m) and c_P is P -wave velocity (m/ms). Note that A_r is not continuous at $\Delta T/T_{\max} = 1$, but replacing the constant term 2.1 by 2.05 would make it so.

As previously stated, the various factors (e.g., the rock description pre-factor 0.06) were tailored by Cunningham to fit the median. The final form of the Kuznetsov–Cunningham formula should be (Cunningham 2005):

$$x_{50} = AA_r q^{-0.8} Q^{1/6} \left(\frac{RWS}{115} \right)^{-19/30} C(A) \tag{8}$$

The factor $C(A)$ is included in order to correct the predicted median size, to be determined experimentally from data in a given site; according to Cunningham, it would normally be within the range $0.5 < C(A) < 2.0$. This suggests a prediction error expected of up to about 100%. This is larger than Kuznetsov’s (1973) error bounds, but while Kuznetsov’s A values lie in the range 7–13, Cunningham (1987) covers the much wider range 0.8–22.

Besides adapting Kuznetsov’s central size formula, Cunningham (1983) followed up the conclusion of the Soviet researchers that the fragmented rock could be described by the RR function and formulated an equation for the uniformity or shape index (n in Eq. 3); in its final form, after several corrections and refinements (Cunningham 1987, 2005), the shape index for the RR distribution of rock fragments is:

$$n = n_s \left(2 - 0.03 \frac{B}{d} \right)^{0.5} \left(\frac{1 + S/B}{2} \right)^{0.5} \left(1 - \frac{W}{B} \right) \left(\frac{l_c}{H} \right)^{0.3} \left(\frac{A}{6} \right)^{0.3} C(n) \tag{9}$$

where W is drilling deviation, l_c is charge length, H is bench height and n_s is a factor that accounts for the delay precision:

$$n_s = 0.206 + (1 - R_s/4)^{0.8}, \quad R_s = 6s_t/\Delta T \quad (10)$$

where s_t is the standard deviation of the initiation system. The factor $C(n)$ is, again, a variable correction to match experimental data if available; no expected range is given to it.¹

The Kuznetsov–Cunningham formula is physically sound, as previously discussed. Similar forms may be obtained applying asteroid collision principles (Holsapple and Schmidt 1987; Housen and Holsapple 1990) as shown by Ouchterlony (2009b). However, the experimental data supporting the median size expression are, as mentioned above, extremely limited. Furthermore, no experimental data supporting the shape index formula seem to have been reported. The initial shape index dependence on geometry appears to originate in 2D blast modeling by Lownds (1983) (Cunningham 1983, p. 441).²

The assessment of the Kuz-Ram model by, e.g., the JKMRC (Kanchibotla et al. 1999; Thornton et al. 2001; Brunton et al. 2001) and other publications (e.g., Ford 1997; Morin and Ficarazzo 2006; Gheibie et al. 2009a, b; Hafsaoui and Talhi 2009; Strelec et al. 2011; Tosun et al. 2014) seldom include hard experimental data and are often obscured by the lack of real knowledge of the resulting muckpile fragmentation, which hinders a reliable error assessment. A generally accepted weakness of the Kuz-Ram model is that it normally predicts too few fines in a muck pile. This led to model extensions involving one RR function for the coarse material and another for the fines, the crush zone model (CZM, Kanchibotla et al. 1999; Thornton et al. 2001; Brunton et al. 2001) and the two-component model (TCM, Djordjevic 1999) from the JKMRC. Of these, the CZM has become the one more used. The CZM rests on the assumption that the fines come from a volume around the borehole in which the rock may fail under compression (it is ‘crushed’); the radius of the crush zone is:

$$r_c = r_b \sqrt{\frac{P_b}{\sigma_c}} \quad (11)$$

where r_b is the borehole radius, P_b is the borehole pressure and σ_c is the uniaxial compressive strength. The crushed volume is a fraction F_c of the volume excavated by each borehole, BHS:

$$F_c = \frac{\pi(r_c^2 - r_b^2)(H - l_s)}{\text{BHS}} \quad (12)$$

where l_s is the stemming length. The crushed zone

¹ The factor $(A/6)^{0.3}$ in Eq. 8 is absent in Cunningham (2005), Eq. 14. This must be a typographical error since this factor is defined in his Eq. 12 and present in his Table 1. The factor $(A/6)^{0.3}$ introduces a weak dependence of n on rock mass conditions.

² As a strong indicator of the source, we take, e.g., Lownds’s Fig. 8. From it follows the term $1 - W/B$ in the n -factor formula.

maximum size of fragments is assumed to be 1 mm. The CZM uses the Kuz-Ram model³ for the coarse part (above 50% passing for competent rock, $\sigma_c > 50$ MPa, and 90% for soft rock, $\sigma_c < 10$ MPa), below which a second RR function is used, defined so as to include (for the competent rock case) the $(x_{50}, 0.5)$ and $(1 \text{ mm}, F_c)$ points; for the soft rock case, the grafting point is $(x_{90}, 0.9)$.⁴ Such a ‘fines’ RR function is defined by x_{50} and a uniformity index n_f :

$$n_f = \frac{\ln\left[-\frac{\ln(1-F_c)}{\ln 2}\right]}{\ln[1/x_{50}(\text{mm})]} \quad (13)$$

An analogous expression can be obtained for the soft rock case.

Both the Kuz-Ram model and its CZM extension have been assessed with the data set of 169 blasts that is described in Sect. 3. Figure 1 shows the logarithmic errors of the size prediction:

$$e_L = \ln\left(\frac{x^*}{x}\right) \quad (14)$$

where x^* and x are predicted and data sizes, respectively.⁵

The error of the Kuz-Ram and crush zone predictions in about half of the cases (the interquartile range) lies within an approximate range $[-0.6, 0.4]$, roughly equivalent to relative errors -75 to $+50\%$ in nearly the whole percentage passing range. The prediction is noticeably negative-biased (the sizes predicted are smaller than the data) in most of the range except the upper end. Other conclusions from Fig. 1 are that the largest bias occurs in the central zone, which suggests that (1) the median size formula has a limited predictive capability in terms of accuracy, with a systematic error of some -30% ; the precision (i.e., the random error around the central value) is also limited, with the interquartile range of about $[-75, +50\%]$; this prediction error is larger than the assessment by Ouchterlony (2016a) on the original Kuznetsov’s formula (-42 to 55% maximum error), though the number of blasts used in the present case more than quadruples the data set used by Kuznetsov; (2) the prediction in the extremes of the range analyzed is somewhat better than in the central range which

³ In what the CZM makes use of the Kuz-Ram formulae, their last versions (Eqs. 6–10, Cunningham 2005) have been used. The CZM contains an in-house redefinition of the rock factor A , which seems to have never been officially published; it is used here in its original form, i.e., Kuz-Ram’s rock factor.

⁴ Kanchibotla et al. (1999) say that ‘It is likely that for intermediate strength rocks the point where the two distributions are joined will vary between x_{50} and x_{90} .’ How this is effected in practical applications has not been published however.

⁵ Note that a log error $\pm \ln 2 = \pm 0.69$ means a prediction value double or half the data value, $\pm \ln 3 = \pm 1.10$ corresponds to triple/one-third, etc.

Fig. 1 Boxplots of the prediction error for the Kuz-Ram and crush zone models, based on the data set of 169 blasts. *Blue boxes* Kuz-Ram; *magenta boxes* CZM. *Horizontal lines* show the $\ln 1.5$ and $-\ln 1.75$ levels, equivalent to relative errors +50 and -75% (color figure online)

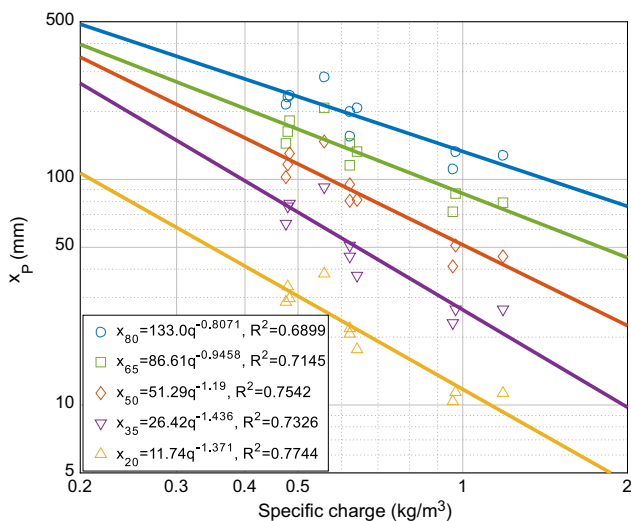
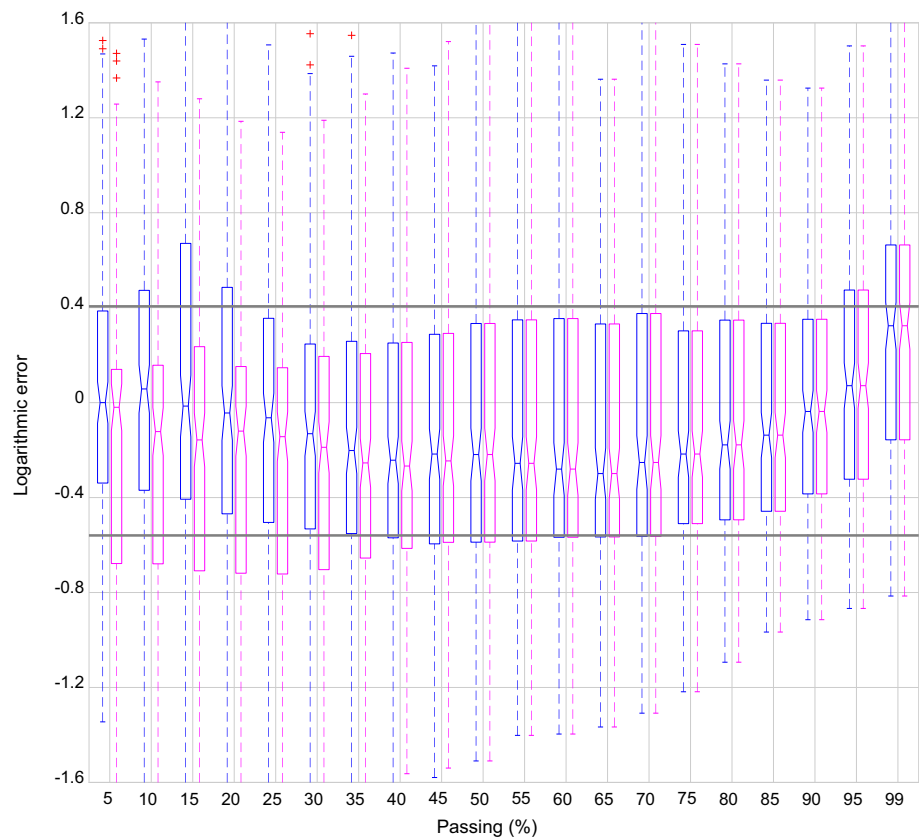


Fig. 2 Log–log interpolated percentile size data x_p for rounds #1, 2, 5, 6, 13, 14, 18, 19, 25, 29 from Otterness et al. (1991) with $P = 20, 35, 50, 65$ and 80% . Fitted power laws $x_p = A/q^k$ are plotted (color figure online)

means that also the uniformity (the overall slope in the size/passing plot in log–log) of the distribution is generally overestimated.

The data from the seminal small-scale (bench height of about 1 m) blasting tests by Otterness et al. (1991)

underscore the above. Plotting some percentile sizes as a function of the powder factor from a selection of 10 blasts of nearly identical geometry gives the results shown in Fig. 2. Power laws fit each percentile size quite well (the determination coefficients are given in the figure; both the pre-factor and the exponent are significant in all the fits, and the maximum p values are 0.002 for the pre-factor and 0.003 for the exponent). Ouchterlony et al. (2016) show that such pattern requires that (1) the RR exponent would need to be variable at different percentiles (which would require a different function—e.g., a piecewise RR with variable exponent), and (2) its value should depend on the specific charge; only if the exponent of the power law $x_p = \text{const}/q^k$ is constant in some percentile interval, then the RR exponent might not depend on q , but it would still need to vary at different percentiles. This fundamental discrepancy with the experimental evidence lies at the core that the RR function with a single n value is a poor description of the fragmentation data, and a severe hindrance for its use in state-of-the-art fragmentation prediction models.

The x_p versus specific charge convergent lines pattern (which we call ‘fan’ plots) is a general characteristic of fragmentation by blasting. In fact, most of the groups of data that form the basis for this work show the same behavior as the data in Fig. 2; power laws fit the percentile size data to the powder factor quite well, and the exponent

is a function of P . In well-controlled model-scale blasts, this behavior is extremely well developed; the consequences of that are discussed in Ouchterlony et al. (2016).

The facts above are not described by any known credible theory of blast fragmentation that favors a specific fragment size distribution. On the contrary, they speak in favor of developing prediction equations for blast fragmentation that do not depend on any specific size distribution function. Size and passing data have a clear physical meaning, whereas shape, or uniformity, indices are just a reduced interpretation of the data through some particular size distribution. A median, or a 20 percentile size, even a 63.2 percentile like x_c , have their full meaning without any additional statement; however, a shape index has no real meaning unless it is tied to a particular distribution—a RR, a Swebrec, a lognormal, a maximum-size-transformed RR one, etc.

2 The Model Foundations

Ouchterlony's (2009b) blasting-related interpretation of Holsapple and coworkers' work on asteroid collisions (Holsapple and Schmidt 1987; Housen and Holsapple 1990) has already been mentioned. From the dimensional analysis, Ouchterlony arrives at the following expression for the fraction P of fragments of mass less than m :

$$P = F_1\left(\frac{m}{M}, \Pi_s, \Pi_g\right) \quad (15)$$

where M is the total nominal mass fractured; Π_s and Π_g are strength- and gravity-related non-dimensional parameters; and F_1 is an unspecified functional dependence.

The mass of a fragment is $m = k_1 \rho x^3$, x being size and k_1 a particle shape factor. The nominal mass broken for each explosive charge, for the case of bench blast, is generally approximated as $M = \rho BHS / \cos \theta$, θ being the holes inclination angle with respect to the vertical. Introducing a (as yet undetermined) characteristic blast size L_c , $M = k_2 r L_c^3$, with k_2 a blast geometry or bench shape factor:

$$k_2 = \frac{BHS}{L_c^3 \cos \theta} \quad (16)$$

Equation 15 becomes:

$$P = F_1\left(\frac{k_1 x^3}{k_2 L_c^3}, \Pi_s, \Pi_g\right) \quad (17)$$

Neglecting the gravity parameter (that, for the case of asteroids, applies to bodies for which the material strength is less than the gravitational self-compressive strength which, obviously, does not apply to Earth) and solving Eq. 17 for x/L_c :

$$\frac{x}{L_c} = F_2\left(P, \frac{k_1}{k_2}, \Pi_s\right) \quad (18)$$

The strength factor Π_s has the following expression (Ouchterlony 2009b, Eq. 7b, adapted from Housen and Holsapple 1990, Eq. 40):

$$\Pi_s = E_M \left(\frac{\sigma^*}{\rho}\right)^{3\mu/(\tau-2)} L_s^{-3\mu(\lambda+\tau)/(\tau-2)} e^{(3\mu-2)/2} \left(\frac{\rho}{\rho_e}\right)^{1-3\nu} \quad (19)$$

where E_M is impact energy per target mass, clearly related to the powder factor in rock blasting; σ^* is a rock strength quantity with dimension [stress][length]²[time] ^{τ} ; e is the explosive energy per unit mass;⁶ ρ_e is impactor density which is transposed in the blasting model as the explosive density;⁷ and L_s is a characteristic length (in the collision model, it is the target radius) that we will choose for simplicity equal to L_c .⁸ The constants μ , ν , λ and τ are to be determined experimentally. μ and ν describe the impactor coupling to the target; the two extremes of the coupling are energy-scaled impacts ($\mu = 2/3$, $\nu = 1/3$) and momentum-scaled ones ($\mu = 1/3$, $\nu = 1/3$). Holsapple and Schmidt (1987) show that the case of a point source explosion has $\mu = 2/3$ and that collisions on non-porous targets, including rocks, are governed by μ close to 0.6, whereas porous targets (such as dry sand) have $\mu = 0.37$ –0.40, close to the momentum limit. Selecting thus the energy-scaled interaction for the blasting case analogy in Earth's rock:

$$\Pi_s = E_M \left(\frac{\sigma^*}{\rho}\right)^{2/(\tau-2)} L_c^{-2(\lambda+\tau)/(\tau-2)} \quad (20)$$

λ and τ are material constants that describe the dependence of the strength on the scale of the target and the loading rate, respectively. Loading rate in blasting can, in principle, be described by the rise time of the pressure in the borehole, or the reaction time in the detonation front. This time is proportional to the ratio of the length of the reaction zone to the average sound speed of the detonation products in the reaction zone (Price 1981); in homogeneous explosives such as straight emulsions, it can range from less than

⁶ The collision model uses impact velocity U , dimensionally equal to the square root of energy per unit mass (hence the dividing factor 2 in the exponent of e that does not exist when U is used). Note that the impact energy per unit impactor mass for a typical collision velocity of some km/s is some MJ/kg, of the same order of magnitude that energies per unit mass of explosives.

⁷ Having equated the velocity squared of the impactor to the explosive energy per unit mass, the density of the impactor plays the same role as the explosive density since, for both, the driving energy is formally density \times volume \times energy per unit mass.

⁸ L_c is also an equivalent block length (actually the edge length of the cube with equal volume); choosing this or an equivalent sphere radius would only mean a different value for the shape factor k_2 .

100 ns to about 1 μs, depending on the size of the sensitizing microspheres (Hirosaki et al. 2002); for heterogeneous explosives such as ANFO or ANFO/emulsion mixtures, rise times in the order of 10 μs have been reported (Onederra et al. 2011). Reaction time, or reaction zone thickness with which to estimate the reaction time using the reaction zone sonic velocity (that can be estimated from the detonation velocity), is never included in blasting reports so we have no way to assess its influence in the model. We are forced then, as a first approximation, to not consider the loading rate dependence, i.e., make $\tau = 0$ in Eq. 20.

About the scale dependence, let us define $\bar{\sigma}$ as the strength (with dimensions of stress) of the rock mass of a certain size \bar{R} ; we may write:

$$\sigma^* = \bar{\sigma} \bar{R}^\lambda \tag{21}$$

Assuming σ^* invariant for a certain rock mass (which amounts to consider a classical power dependence of strength with size, Persson et al. 1994, quoting Weibull 1939; Jaeger and Cook 1969; Hoek and Brown 1980; Scholz 1990), the strength for a given size R is:

$$\sigma = \frac{\bar{\sigma}}{(R/\bar{R})^\lambda} \tag{22}$$

Using Eq. 21 for σ^* and making $\tau = 0$ in Eq. 20 for a non-rate variable model:

$$\Pi_s = E_M \left(\frac{\bar{\sigma} \bar{R}^\lambda}{\rho} \right)^{-1} L_c^\lambda \tag{23}$$

Writing E_M (energy per unit rock mass) in terms of the powder factor q (mass of explosive per unit rock volume) and the explosive energy per unit mass e , $E_M = qe/\rho$, the factor Π_s becomes:

$$\Pi_s = \frac{qe}{\bar{\sigma}} \left(\frac{L_c}{\bar{R}} \right)^\lambda \tag{24}$$

The size of fragments for a given fraction passing P , or size quantile P , becomes, from Eq. 18:

$$\frac{x}{L_c} = F_2 \left[P, \frac{k_1}{k_2}, \frac{qe}{\bar{\sigma}} \left(\frac{L_c}{\bar{R}} \right)^\lambda \right] \tag{25}$$

The Kuznetsov formula and others that have been proposed for the calculation of the fragments size (Langefors and Kihlström 1963; Holmberg 1974; Larsson 1974; Kou and Rustan 1993; Rustan and Nie 1987) generally agree that the central fragment size is a power function of the powder factor; plots as the ones in Fig. 2 say the same for other percentile sizes so this will be attempted here. Assuming a power form also for the other parameters and writing Π_s and the k -ratio as the reciprocals in Eq. 25, this becomes:

$$\frac{x}{L_c} = P^r \left(\frac{k_2}{k_1} \right)^h \left(\frac{\bar{\sigma} \bar{R}^\lambda}{qe L_c^\lambda} \right)^\kappa = P^r \left(\frac{k_2}{k_1} \right)^h \left(\frac{\bar{\sigma}}{qe} \right)^\kappa \left(\frac{\bar{R}}{L_c} \right)^{\lambda \kappa} \tag{26}$$

The constants r , h , κ and λ are to be determined from experimental data. Note that they are not universal for all percentages passing since that would lead to a Gates–Gaudin–Schuhmann distribution (Gates 1915; Gaudin 1926; Schuhmann 1940), with exponent $1/r$:

$$P = \left(\frac{x}{x_{\max}} \right)^{1/r}; \quad x_{\max} = \left(\frac{k_2}{k_1} \right)^h \left(\frac{\bar{\sigma}}{qe} \right)^\kappa L_c^{1-\lambda \kappa} (\bar{R})^{\lambda \kappa} \tag{27}$$

The P -dependence of κ is already stated in Sect. 1 (Fig. 2), and the variation of r follows from the fact that the log–log slope of the cumulative size distribution is known to vary across the percentage passing range. In fact, Eq. 27 could be thought of as a piecewise log–log linear representation of the size distribution in which the top size and the slope vary constantly across the size range.

The fragments shape factor k_1 is an experimental variable that is generally unknown so it will be considered as one more parameter (that, in principle, may also vary with the size of the fragments, hence with the percentile). Thus, for each percentage passing P , the group P^r/k_1^h can be considered a single parameter, k (which should tend to zero with P). Assuming arbitrarily that the strength parameter $\bar{\sigma}$ corresponds to a unit size (in the same units as those used for L_c) of rock mass, $\bar{R} = 1$, Eq. 26 is, finally:

$$\frac{x_P}{L_c} = k k_2^h \left(\frac{\bar{\sigma}}{qe} \right)^\kappa \frac{1}{L_c^{\lambda \kappa}} \tag{28}$$

The size has been written x_P to show that it is the percentile P size. This model requires the calibration of the four functions $k(P)$, $h(P)$, $\kappa(P)$ and $\lambda(P)$ which, together with the selection of the strength variable $\bar{\sigma}$ and the characteristic size L_c , will be accomplished from experimental data.

3 The Data

Fragmentation data from bench blasting have been gathered for a total of 169 blasts published in the literature. Some of them were small-scale (half to 1 m bench height) tests, and others were full-scale production blasts; all of them were carried out in the field on natural rock mass. For all of them, the fragmentation data were obtained by sieving and weighing of a sample of the muckpile, and the description of the blasts and the rock mass was reasonably detailed so that calculations of the Kuz-Ram type made in Sect. 1, and likewise of the model presented here, can be carried out. Table 1 lists the mine and quarry sites and the sources of the data; Table 2 gives a general description of

Table 2 Fragmentation data

Blast site	No. blasts	n_p	x_{\min} (mm)	x_{\max} (mm)	P_{\min} (%)	P_{\max} (%)	Amount sieved	
							t per blast	%
El Alto, Spain	1	14	0.1	1500	0.017	100	481	2
Mt. Coot-tha, Australia	1	5	5.0	1000	2.5	100	32	0.05
Bårarp, Sweden	7	19–20	0.075	500–1000	0.1–0.6	47.9–98.7	247–490	100
Kållerred, Sweden	6	17	0.075	2000	0.34–0.49	100	3660–5638	100
Billingsryd, Sweden	6	19	0.074	2360	0.76–1.03	100	10,087–12,898	100
Rolla, MO, USA (Otterness et al.)	29	6–8	9.525	229–457	7.9–20.6	100	0.5–10.5	100
High Forest, MN, USA	20	7–8	4.7625	229–559	1.03–3.86	100	0.9–2.0	100
Guan Shan, China	8	11	100	1500	4.7–11.4	100	4.3–9.3	100
Rolla, MO, USA (Stagg and Nutting)	18	7–8	4.7625	304.8–609.6	2.8–7.4	100	0.7–2.8	100
Waterloo, IA, USA	7	4–5	31.8–57.15	608–738	18.4–27.5	89.4–95.3	141–730	11–100
St Paul Park, MN, USA	6	5	31.8	562–584	27.5–30.7	96.7–97.9	92–270	34–100
Granite Falls, MN, USA	3	5	31.8	543–579	22.8–31.7	96.9–99.2	280–413	3–5
Manitowoc, WI, USA	6	5	22.2	653–825	17.9–22.4	89.8–95.5	130–325	5.5–13
Vändle, Sweden	4	19	0.063	1000	0.50–1.11	100	98–122	0.6–0.9
Långåsen, Sweden	6	19	0.063	1000	0.78–1.10	100	94–413	0.5–1.1
Rolla, MO, USA (Smith)	20	7	4.7625	304.8	1.7–9.7	48–89.5	0.4–2.4	100
Rolla, MO, USA (Brinkmann)	13	7	4.7625	304.8	2.24–7.20	65.1–90.2	1.2–2.8	100
Rolla, MO, USA (Bleakney)	8	7	4.7625	304.8	1.56–7.7	74.1–94.3	1.6–3	100

n_p , no. of data points per curve; x_{\min} , x_{\max} , minimum and maximum size (where P_{\max} is not 100%, x_{\max} is a log–log extrapolated value to $P = 100\%$); P_{\min} , P_{\max} , minimum and maximum percentage passing

Table 3 Rock properties

Blast site	Density (kg/m ³)	E (GPa)	σ_c (MPa)	c_p (m/s)	s_j (m)	j_o	$\sigma_c^2/(2E)$ MPa	RMD	A
El Alto, Spain	2560	64	119	2994	2.4	0.25	0.11	J	7.7
Mt. Coot-tha, Australia	2730	82.5	200	5766	0.5	0.75	0.24	J	10.1
Bårarp, Sweden	2660–2670	82.5	237	5525	4.0	0.5	0.34	M	6.8–6.9
Kållerred, Sweden	2690	34.5	168	5525 ^a	0.47	1.0	0.41	J	8.9
Billingsryd, Sweden	2945–2972	44.7	252	4088–4107 ^a	0.97	0.75	0.71	J	8.9–9.0
Rolla, MO, USA	2650–2677	15.0	62	4496–4511	0.29	0.25	0.13	J	3.1
High Forest, MN, USA	2700	50.0–55.7	143–155	5742–5766	0.10	0.25	0.20–0.21	J	3.8–4.7
Guan Shan, China	2560	27.0	112	3896	1.5	1.0	0.23	M	4.4
Waterloo, IA, USA	2674–2701	57 ^a	131 ^a	3208–3922	0.53	0.25	0.15	J	8.0
St Paul Park, MN, USA	2677 ^a	15 ^a	62 ^a	2228–3627	0.34	0.25	0.13	J	6.7
Granite Falls, MN, USA	2670 ^a	36 ^a	166 ^a	4420 ^a	0.20	0.5	0.38	J	4.1
Manitowoc, WI, USA	2677 ^a	15.0 ^a	62 ^a	3050 ^a	2.0	0.25	0.13	M	4.3
Vändle, Sweden	2640	70.3	207	5612	0.5	0.75	0.31	J	10.0
Långåsen, Sweden	2677	67	206	5275	0.75–4.5	0.5	0.32	J	7.7–9.5
Overall range	2560–2972	15.0–83.0	62–252	2228–5766	0.10–4.5	0.25–1.0	0.11–0.71	J–M	3.1–10.1

E , Young's modulus; σ_c , uniaxial compressive strength; c_p , longitudinal wave velocity; s_j , mean joint spacing; j_o , joint orientation index (as defined in Sect. 4); RMD, Kuz-Ram's rock mass description (J: jointed, M: massive); A , Kuz-Ram's rock factor (Eq. 6)

^a Not reported in the sources; values estimated

the size distribution data; Tables 3, 4 and 5 give relevant rock and blast design variables.

Elastic modulus is sometimes reported in the sources as from laboratory tests (static), and sometimes as calculated

from P- and S-wave velocities, which results in somewhat different figures; the original value quoted in each case has been retained. This adds some uncertainty, or unwanted variability, to the data, that would probably not be

Table 4 Blast design data. Explosives and initiation systems

Blast site	Explosive type ^a	Density (g/cm ³)	VOD (m/s)	<i>e</i> (MJ/kg)	<i>Q</i> (kg)	<i>q</i> (kg/m ³)	<i>qe</i> (MPa)	Δt (ms)	Detonator type
El Alto, Spain	ANFO-Al	0.8	4029	4.84	224	0.45	2.18	42	Non-el
Mt. Coot-tha, Australia	Watergel	1.2	5447	4.01	119	0.52	2.08	25	Non-el
Bårarp, Sweden	Emulsion	1.2–1.225	5000–5851	1.27 ^b –3.20	5.5–19	0.42–0.47	0.59–1.51	25	Electronic
Kållerød, Sweden	Emulsion	1.3 ^c	2707–5470	2.90	45–54	0.46–0.63	1.34–1.82	42	Non-el
Billingsryd, Sweden	Emulsion	1.3 ^c	3234–5638	2.90	109–157	0.69–0.84	1.99–2.43	25–42	Non-el
Rolla, MO, USA	Dynamite	1.12	2560	2.94	0.05–1.1	0.43–1.22	1.26–3.57	1.7–5.8	Seismic ^d
High Forest, MN, USA	Dynamite	1.12	2560	2.94	0.05–0.07	0.23–0.51	0.69–1.50	0–25	Electric
Guan Shan, China	Dynamite	0.93	3010	1.76 ^b	0.52	0.67	1.17–1.18	0–1.9	Non-el ^e
Rolla, MO, USA	Dynamite	1.12	2560	2.94	0.14	0.43–0.62	1.27–1.82	0–45	EBW ^f
Waterloo, IA, USA	ANFO, Emulsion, Dynamite	0.81–1.34	3840–5578	2.94–3.89	28–39	0.42–0.57	1.32–1.91	12	Electronic
St Paul Park, MN, USA	Dynamite	1.12	4330	2.94	12.2	0.50–0.51	1.48–1.49	2–48	Seismic ^d
Granite Falls, MN, USA	ANFO, Emulsion	0.8–1.15	4000–4830	3.27–3.89	102–173	0.72–1.05	2.79–3.76	10–12	Electronic
Manitowoc, WI, USA	ANFO, Emulsion	0.8–1.2	3800–4830	3.27–3.89	39–56	0.75–1.00	2.92–3.51	13	Electronic
Vändle, Sweden	Emulsion	1.17–1.23	4718–4771	3.34	77–93	0.53–0.76	1.77–2.53	42	Non-el
Långåsen, Sweden	Emulsion	0.98–1.15	5110	3.25	85–116	0.72–1.05	2.35–3.43	5–25	Non-el, Electronic
Rolla, MO, USA (Smith)	Dynamite	1.12	2560	2.94	0.03–0.14	0.44–1.00	1.30–2.95	0–25	Electric
Rolla, MO, USA (Brinkmann)	Dynamite	1.12	2560	2.94	0.14	0.41–1.00	1.22–2.95	0–25	Electric
Rolla, MO, USA (Bleakney)	Dynamite	1.12	2560	1.38 ^b –2.94	0.14–0.19	0.45–0.65	0.80–1.91	25	Electric
Overall range		0.8–1.34	2560–5851	1.27–4.84	0.03–224	0.23–1.22	0.59–3.76	0–48	

VOD, detonation velocity; *e*, specific explosive energy (per unit mass); *Q*, charge per hole; *q*, powder factor or specific charge; *qe*, energy powder factor or explosive energy concentration; Δt , in-row delay

^a Emulsion designates both straight and blend products

^b Decoupled charges. Decoupling ratios (hole-to-charge diameter ratio): Bårarp 1.5, Guan Shan 1.31, Rolla (Bleakney): 1.06–1.5 (energy of the decoupled shots 2.61–1.38 MJ/kg)

^c Mean charge density (includes dynamite as bottom charge, density 1.45 g/cm³)

Precisions for nonstandard systems (not reported for electric, non-electric or electronic)

^d 0.11 ms

^e The delay was given by different lengths of shock tube

^f Exploding bridge wire. Precision: max (0.0025% delay time, 50 ns)

overcome very much by the estimation of one from the other by grossly approximate formulae (e.g., Eissa and Kazi 1988). In some cases, some properties have been estimated from the data available using, e.g., elastic relations or properties of similar rocks. These are marked in Table 3.

The explosive energy is rated as the heat of explosion value, both for it being a well-defined magnitude, that

does not depend much on the detonation thermodynamic code and on the products expansion assumptions, and for being a property commonly specified by the manufacturers; this is the same approach as the Kuz-Ram model in which the explosive energy is rated by means of the relative weight strength, a measure of the heat of explosion with respect to ANFO. Other explosive energy values such as the useful work could indeed be used, but the

Table 5 Blast design data. Other dimensional and non-dimensional parameters

Blast site	d (mm)	B (m)	H (m)	S (m)	l_c (m)	S/B	\sqrt{HS}^a (m)	$c_P \Delta t / S^b$	$\frac{B}{\sqrt{HS} \cos \theta}^c$	No. rows
El Alto, Spain	142	5.00	18.6	6.00	15.8	1.20	10.56	21.0	0.48	1
Mt. Coot-tha, Australia	102	3.80	14.0	4.30	12.1	1.13	7.76	33.5	0.46	4
Bårarp, Sweden	38–76	1.35–2.70	5.0–5.3	1.65–3.40	3.7–4.4	1.17–1.26	2.93–4.12	40.6–83.7	0.46–0.66	1
Kållerred, Sweden	76	2.60–2.90	8.6–9.8	2.9–3.3	5.5–8.4	1.00–1.23	5.22–5.69	70.3–80.0	0.49–0.58	3
Billingsryd, Sweden	76	2.60–3.00	16.4–19.5	2.8–3.2	16.8–19.2	1.03–1.19	7.13–7.90	50.8–88.1	0.35–0.43	3
Rolla, USA (Otterness)	11–25	0.25–0.76	0.43–2.26	0.34–1.07	0.4–1.9	1.00–2.03	0.48–1.55	12.4–59.0	0.34–0.79	1
High Forest, MN, USA	22	0.36–0.44	0.70–0.90	0.38–0.88	0.3–0.5	1.00–2.00	0.56–0.84	0–378.3	0.48–0.68	1
Guan Shan, China	42	0.43–0.75	1.4	0.75–1.30	0.7	1.00–3.02	1.02–1.35	0–9.9	0.32–0.73	1
Rolla, USA (Stagg and Nutting)	27	0.38	1.14	0.53–0.76	1.0	1.40–2.00	0.78–0.93	0–379.3	0.41–0.49	1
Waterloo, IA, USA	89	1.98	6.71	3.05	4.7–5.2	1.54	4.52	12.6–15.4	0.44	1, 3
St Paul Park, MN, USA	63.5	1.75	6.71	2.06	4.9	1.17	3.71	3.0–71.3	0.47	1
Granite Falls, MN, USA	140	3.05–3.35	11.3–12.8	3.96–4.88	8.3–9.8	1.30–1.46	6.69–7.90	10.8–11.2	0.42–0.46	3
Manitowoc, WI, USA	89	1.98	8.23	2.99–3.20	7.2–7.3	1.52–1.62	4.96–5.13	12.4–13.3	0.39–0.40	3
Vändle, Sweden	90	2.86–3.46	10.8–12.7	3.71–4.27	10.3–12.0	1.21–1.34	6.58–7.22	55.2–63.5	0.43–0.52	4
Långåsen, Sweden	89	2.16–2.55	12.9–16.7	2.9–3.4	12.9–16.6	1.33–1.35	6.12–7.54	7.8–45.5	0.32–0.38	4
Rolla, USA (Smith)	27	0.26–0.48	0.38–1.14	0.38–0.76	0.25–1.0	0.79–2.65	0.38–0.93	0–296	0.31–1.26	1
Rolla, USA (Brinkmann)	27	0.34–0.38	1.14	0.38–0.76	1.0	1.00–2.08	0.66–0.93	0–296	0.39–0.58	1
Rolla, USA (Bleakney)	15.9–19	0.35–0.41	1.14–1.45	0.57	1.0–1.3	1.41–1.64	0.81–0.91	197	0.38–0.50	1
Overall range	11–142	0.25–5.00	0.38–19.5	0.34–6.00	0.25–19.2	0.79–3.02	0.38–10.6	0–379.3	0.31–1.26	1–4

d , hole diameter; B , burden; H , bench height; S , spacing; l_c , charged length

^a Characteristic length L_c in the model

^b Non-dimensional delay factor Π_l in the model

^c Bench shape factor k_2 in the model

model would require a recalibration with them—a difficult task though, since useful work is often not given by the manufacturers and there is not a common ground for a standard calculation of it. When a heat of explosion value is not reported in the blast description, a value compatible with the type of explosive used has been assigned. In a few cases (9 blasts, their energies marked with b in Table 4), decoupled charges were used; for these, the explosive energy used is the energy remaining in an isentropic expansion point at the expansion ratio equal to the ratio of the borehole volume to the charge volume. This energy has been calculated from the JWL isentropes determined in Sanchidrián et al. (2015) from cylinder test data for ANFO and emulsion-type explosives. Figure 3 shows the ‘energy efficiency,’ or the ratio of the remaining energy at a given expansion (described as decoupling ratio, hole-to-charge diameter ratio) to the energy at expansion ratio equal one (the fully coupled case). Except for some outlier, most of the expansion energy ratio curves are packed in a fairly narrow band so

that, as a first estimation, the mean curve has been used for all decoupled shots (even for the case of dynamite for which no experimental expansion data are available).

4 Model Fitting

For each blast, the fragmentation data have been interpolated to determine the size percentiles between 5 and 100. Linear interpolation in log–log space has been used. Extrapolation has been allowed whenever the range of data does not cover the 5–100% passing; however, a penalty has been applied to the extrapolated points in the fit so that their weight decreases as the extrapolation distance gets longer. The penalty function used is:

$$w_e = e^{-0.5(r_P-1)^3} \quad (29)$$

r_P being the extrapolation ratio:

$$r_P = e^{|\ln(P/P_f)|} \quad (30)$$

Fig. 3 Fraction of energy remaining in the detonation products along expansion

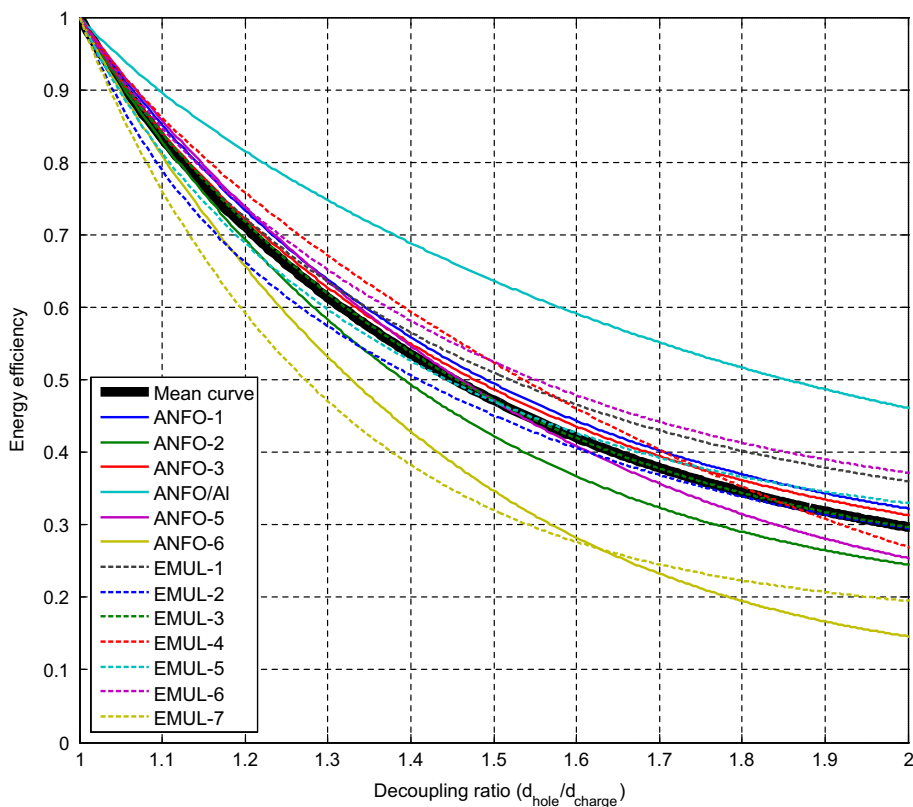


Table 6 Number of extrapolated points

P (%)	100	90	80	70	60	50	40	30	20	10	5	1
No. of interpolated data points	99	122	141	161	164	166	169	167	149	125	96	26
No. of extrapolated points	70	47	28	8	5	3	0	2	20	44	73	143
No. of extrapolated points with $r_p > 2$	3	0	0	0	0	0	0	0	0	20	44	126

where P is the percentage passing at which the size is being calculated and P_f is the lowermost (if $P < P_f$) or uppermost (if $P > P_f$) passing value with data.⁹ The minimum and maximum percentage passing for the different data groups that are listed (P_{min} and P_{max}) in Tables 2 and 6 gives the number of extrapolated points for each percentage passing; the large amount of extrapolated points below $P = 5\%$, with long extrapolations required, prevent from analyzing any lower percentile size.

Besides the extrapolation penalty, a size-dependent weight $w_x = 1/(x/L_c)^{1/2}$ has been included in the least squares scheme, in order to allow a fair influence of the small data and to prevent the larger numbers to be too dominant in the overall error, while not penalizing the determination coefficient too much. The final weight of

⁹ For example, if the lower size data of a distribution are at $P_f = 20\%$, then the value extrapolated at $P = 10\%$ has $r_p = 2$, and a weight $w_e = 0.607$; the value extrapolated at $P = 5\%$ has $r_p = 4$ and $w_e = 1 \times 10^{-6}$.

each point is the smaller of the size-dependent weight (normalized to one) and the extrapolation penalty factor:

$$w = \min(w_e, w_x) \tag{31}$$

Equation 28 is fitted to the x_p data values¹⁰ by means of a Levenberg–Marquardt (Seber and Wild 2003) nonlinear least squares method programmed in a MATLAB (2015) environment. Numerous minimizations (up to 1000 times the number of unknown parameters, and more than that in some particularly difficult cases) are run with variable starting parameters values until the minimum sum of squares is ensured, this way avoiding local minima as much as possible. The result for the 50 percentile sizes of the

¹⁰ For each fit job, we have 169 data points (one from each fragmentation curve i.e. a blast). In principle, none of them is a measured value, but an interpolated one (or extrapolated if this is the case) at the relevant percentage. This way we can combine the data (available from each data set at different percentages passing) into a single percentile set of values. This adds an interpolation error to the experimental uncertainty of the data; this matter is revisited in Sect. 5.

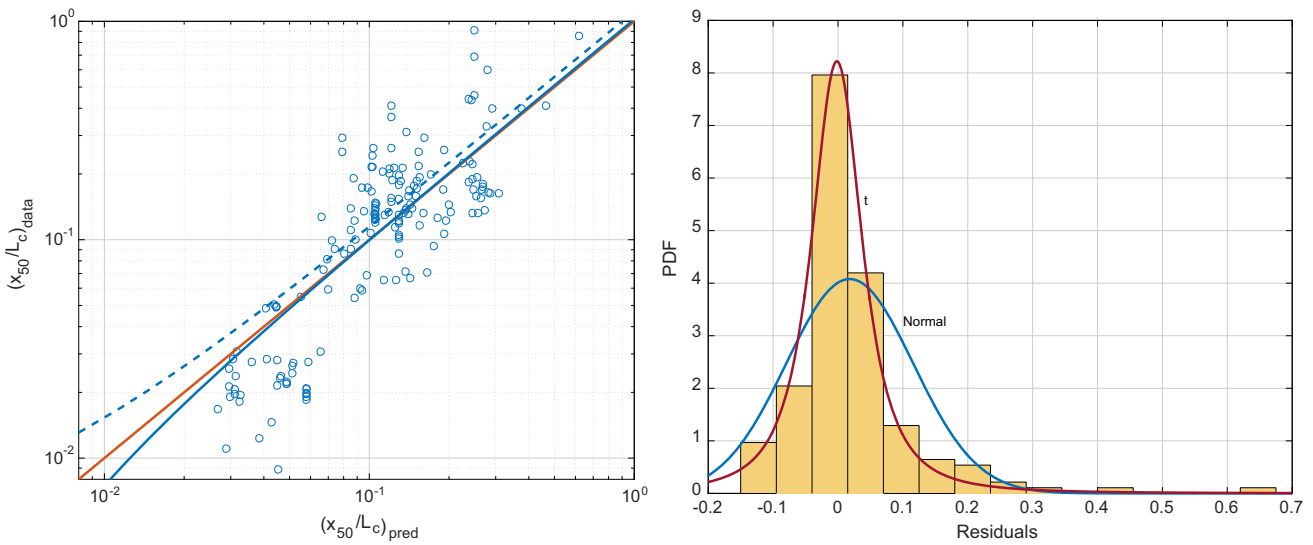


Fig. 4 Four-parameter model (Eq. 28) for x_{50} . *Left* data versus predicted values plot; the *blue lines* are the data versus predicted linear fit (*dashed* ordinary least squares, *solid* robust, least sum of absolute residuals); the *orange line* is the data = predicted values

distributions data is a modest determination coefficient, $R^2 = 0.6413$.

Since the determination coefficient may be a misleading value in nonlinear regression, the relative root-mean-squared error (RRMSE) and the median absolute log error (MALE) are also used as meaningful goodness-of-fit values, as they estimate the prediction capability of the model. The RRMSE is:

$$RRMSE = \sqrt{MSE}/\text{mean}(x_P/L_c) \tag{32}$$

MSE being the mean-squared error:

$$MSE = \frac{1}{n_c - p} \sum_{i=1}^{n_c} w_{ei} [(x_{P,\text{pred}}/L_c)_i - (x_{P,\text{data}}/L_c)_i]^2 \tag{33}$$

n_c being the number of data points (i.e., the number of blasts) and p the number of parameters. The extrapolation weights w_{ei} are applied so that only errors of long extrapolated (hence dubious) points are downsized; the fit weights w from Eq. 31 are not used so as not to give an unrealistic low value of the error. Let the logarithmic error of each predicted value be:

$$e_{Li} = w_{ei} \ln \left(\frac{(x_{P,\text{pred}})_i}{(x_{P,\text{data}})_i} \right) \tag{34}$$

where the extrapolation weights w_{ei} are also applied here. The median absolute log error, MALE, expressed as relative error for better interpretation, $MALE_r$, is:

$$MALE_r = \exp(\text{median}|e_{Li}|) - 1 \tag{35}$$

Both RRMSE and MALE indicate the relative deviation of the predicted values, MALE being more robust (since it is

line. *Right* normalized histogram of residuals; the two PDF functions shown are normal (*blue*) and *t* (*red*), fitted to the distribution of residuals (color figure online)

a median) and symmetric with respect to zero.¹¹ However, high RRMSE may indicate a large number of badly predicted cases (outliers) which may stay hidden with the MALE.

For the fit under study (Eq. 28, x_{50}), $RRMSE = 0.6730$, $MALE_r = 0.4498$. Although the determination coefficient and the errors are mediocre, the parameters of the model ($k = 0.5932$, $h = 1.2029$, $\kappa = 0.2979$, $\delta = 1.7740$) are statistically significant with narrow confidence intervals, p values 8×10^{-7} , 6×10^{-10} , 1×10^{-4} and 2×10^{-4} , respectively. Figure 4 shows the predicted values versus data plot and the distribution of residuals; the latter shows some positive skew, highlighted by the normal and t distributions fitted. The mean is 0.018 and the 95% coverage interval is $[-0.119, 0.256]$. In summary, the model, effectively, translates a significant relation between the variables, but there must be other factors of variation that are not accounted for.

At least two influential characteristics that are relevant to rock blasting are missing from Eq. 28, since they do not apply to asteroid collisions:

1. *The rock mass discontinuities* The important geotechnical information is neither included in the bench shape factor k_2 nor in the fragments shape factor k_1 . Using a classical approach (Lilly 1986, 1992; Scott 1996), the discontinuities are described by means of a combination of a spacing J_s and an orientation J_o term:

¹¹ A predicted value ten times the data value has the same log error as a predicted value one tenth (though with opposite sign), while relative errors for that case are 9 and -0.9 ; this downsizing of the negative errors prevents a fair statistics with relative errors.

$$J_F = J_s + J_o \tag{36}$$

The joint spacing term is formulated as a non-dimensional ratio s_j/L_j , where s_j is the discontinuity mean spacing and L_j a characteristic size, selected as the variable (with dimensions of length) giving a higher determination for the model (see the end of this section). A limiting value a_s is required for large joint spacing:

$$J_s = \min\left(\frac{s_j}{L_j}, a_s\right) \tag{37}$$

The joints orientation term J_o is defined as:

$$J_o = a_o j_o \tag{38}$$

where j_o is Lilly’s joints orientation index normalized to one (listed in Table 3) in order to give it, in principle, a similar weight as the spacing term, though the relative importance of each one will be finally cast by the constant a_o , to be determined from the data. The joints orientation term describes the relative difficulty of the blast to break the toe for different joint orientations with respect to the face: $j_o = 0.25$ (horizontal), 0.5 (dipping out of the face), 0.75 (sub-vertical striking normal to the face) and 1 (dipping into the face or no visible jointing).

2. *The delay* Unlike asteroid collisions, rock blasting is carried out in multiple loadings taking place at successive times for neighboring shots so that there is wave and crack growth interference in the rock mass between two shots in the firing sequence. The general blasting knowledge, confirmed with experimental evidence, states that fragmentation improves (i.e., the size of the fragments decreases) when time is allowed for the cracks from a hole to propagate and damage the rock before the next hole detonates (Winzer et al. 1983; Katsabanis and Liu 1996; Cunningham 2005, referring data by Bergmann et al. 1974; Katsabanis et al. 2006, 2014; Johansson and Ouchterlony 2013). The time for the cracks to propagate is a function of their velocity and that is often normalized by dividing by the P-wave velocity c_p (Roberts and Wells 1954; Dulaney and Brace 1960). In linear elastic materials, the theoretical upper limit of the crack velocity is the Rayleigh wave velocity (Freund 1972), which lies around 90% of the shear wave velocity, though measured crack speeds in rock are hardly in excess of half that velocity (Daehnke et al. 1996; Fourney 2015). Physically, the P-wave velocity determines the time of the first wave arrival from a neighboring blast hole; its use is convenient since, unlike the Rayleigh wave velocity (or the more difficult to know crack velocity), it is a commonly available, easy to determine

and often reported, property for a given rock mass. Thus, the non-dimensional delay factor is defined as:

$$\Pi_t = \frac{c_p \Delta t}{L_t} \tag{39}$$

where Δt is the in-row delay and L_t is a characteristic length (to be selected with the same criterion as the other characteristic lengths, L_c and L_j , see the end of this section).¹² Π_t indicates how large the drill pattern (represented by the characteristic size L_t) is with respect to the travel distance of the longitudinal waves during a delay period. With Π_t defined by Eq. 39, a power form for it cannot hold since it would lead to a zero size for an instantaneous blast if the exponent is positive, or infinite if negative (as should be since the fragment size diminishes with increasing delay). A suitable form of the Π_t function could be an exponential:

$$f_t(\Pi_t) = e^{-\delta \Pi_t} \tag{40}$$

Inserting now the discontinuities term in Eq. 28:

$$\frac{x_p}{L_c} = k \left[\min\left(\frac{s_j}{L_j}, a_s\right) + a_o j_o \right] k_2^h \left(\frac{\bar{\sigma}}{q_e}\right)^k \frac{1}{L_c^{\lambda k}} \tag{41}$$

When Eq. 41, a six-parameter function, is fitted to x_{50} , the determination coefficient grows to $R^2 = 0.8504$, and the other two goodness-of-fit parameters reduce to $RRMSE = 0.4270$, $MALE_r = 0.1873$, all coefficients significant (maximum p value 5×10^{-4}). Inserting now the delay term, Eq. 40:

$$\frac{x_p}{L_c} = k \left[\min\left(\frac{s_j}{L_j}, a_s\right) + a_o j_o \right] k_2^h \left(\frac{\bar{\sigma}}{q_e}\right)^k \frac{1}{L_c^{\lambda k}} f_t(\Pi_t) \tag{42}$$

$R^2 = 0.8549$, $RRMSE = 0.4141$, $MALE_r = 0.2116$, all coefficients significant. The improvement of the quality figures is marginal considering the increase in one parameter of the model ($MALE_r$ even increases). This, together with a moderately high p value for δ (though still within the 0.05 limit, $p = 0.015$), could indicate that the exponential may not be the right form for the delay factor.

If the ratios x_{data}/x_{pred} of Eq. 41 (the function without a delay term) are plotted against Π_t , the result is that of Fig. 5 (left graph); the aspect of this plot suggests a time function decreasing with the time factor down to a minimum, beyond which the function grows toward a constant value. Previous published work supports this behavior (Cunningham 2005, referring to data by Bergmann et al. 1974; Katsabanis et al. 2006, 2014; Johansson and Ouchterlony 2013; Katsabanis and Omidi 2015), though the existence of either a minimum or a lower asymptote is somewhat controversial (Katsabanis

¹² Note that this non-dimensional form of the delay does not differ much from Cunningham’s (2005) $\Delta t/T_{max}$, where the characteristic length is the burden.

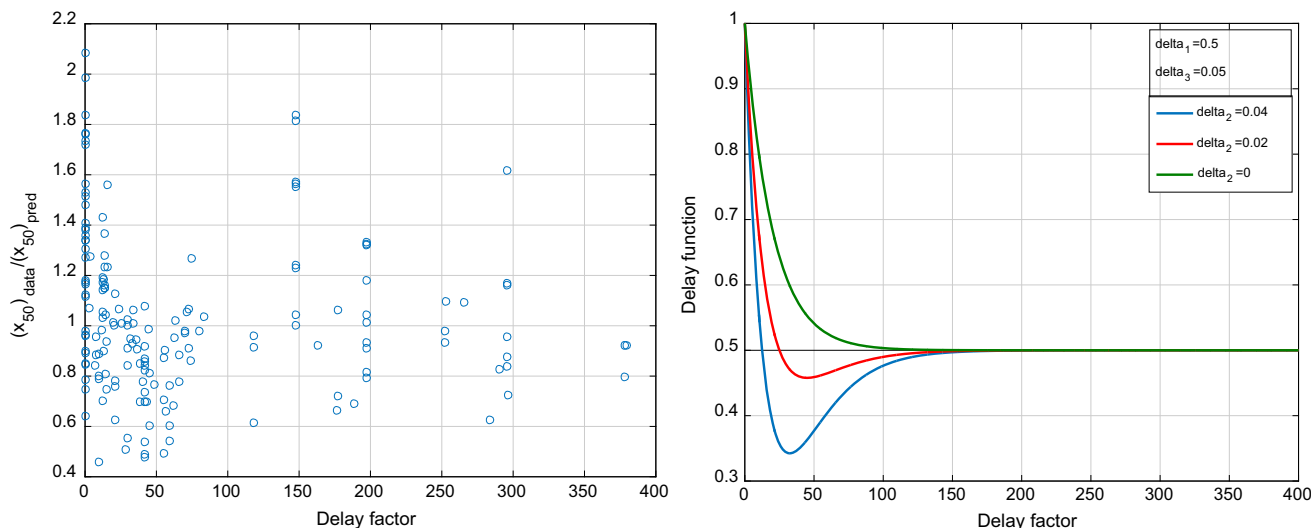


Fig. 5 Left error ratios of a model without delay factor (Eq. 41). Right Sample delay factors as in Eq. 43

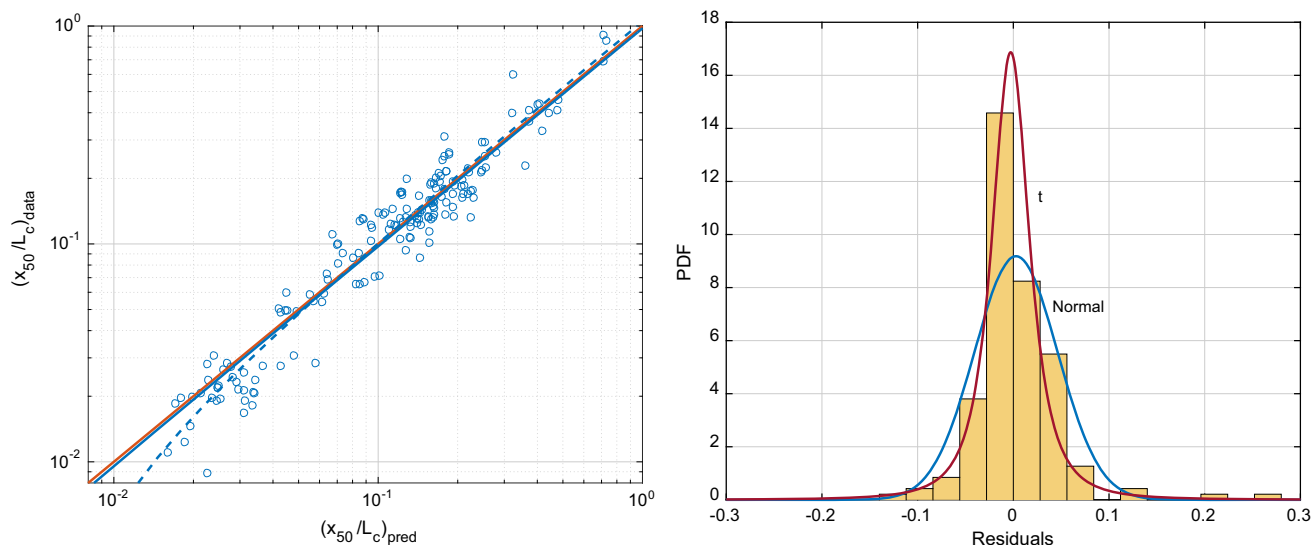


Fig. 6 Nine-parameter model (Eq. 41 with delay function Eq. 43) for x_{50} . Left data versus predicted values plot; the blue lines are data versus predicted linear fits (dashed ordinary least squares, solid robust, least sum of absolute residuals); the orange line is the

data = predicted values line. Right normalized histogram of residuals; the two PDF functions shown are normal (blue) and t (red), fitted to the distribution of residuals (color figure online)

and Omidi 2015 suggest a minimum for the median size, though not so for the 20 percentile). Consequently, a time function has been sought that decreases with increasing delay with the possibility of having a minimum. Such function can be the following:

$$f_t(\Pi_t) = \delta_1 + (1 - \delta_1 - \delta_2 \Pi_t) e^{-\delta_3 \Pi_t} \tag{43}$$

δ_1 , δ_2 and δ_3 being constants to be determined from the fit; $f(\Pi_t)$ is 1 at $\Pi_t = 0$ (the case of simultaneous initiation of holes), decreases to a minimum at $\Pi_t = 1/\delta_2 + 1/\delta_3 - \delta_1/\delta_2$ and then grows toward an asymptotic value δ_1 for long delays (see Fig. 5, right). Equation 43 can also represent a

decay toward a lower asymptote at δ_1 without a minimum if $\delta_2 = 0$, see Fig. 5 (right). Using this delay function leads to $R^2 = 0.9242$, $RRMSE = 0.2992$, $MALE_r = 0.1840$, the nine coefficients strongly significant: the highest p value is 2×10^{-4} . Such low p values (lower than those for Eq. 41, having increased the number of parameters by three) are an outstanding result, a consequence of the narrow confidence intervals of the coefficients, and speak strongly in favor of the delay function in Eq. 43. Figure 6 (left) shows the predicted values versus data plot; Fig. 6 (right) shows the histogram of residuals with normal and t distributions superimposed. The distribution is nearly zero-centered and

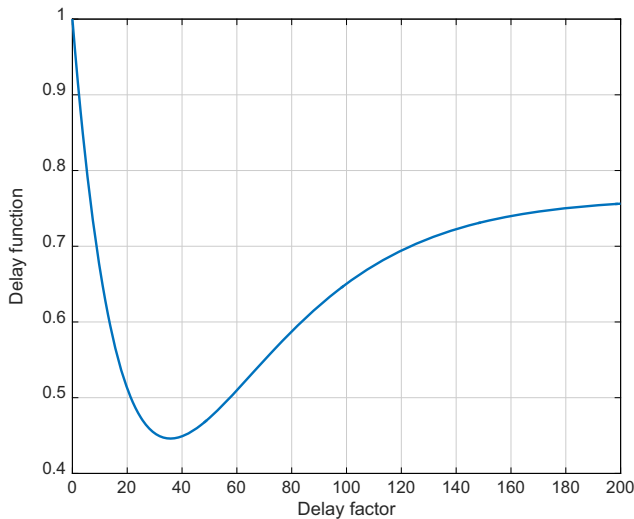
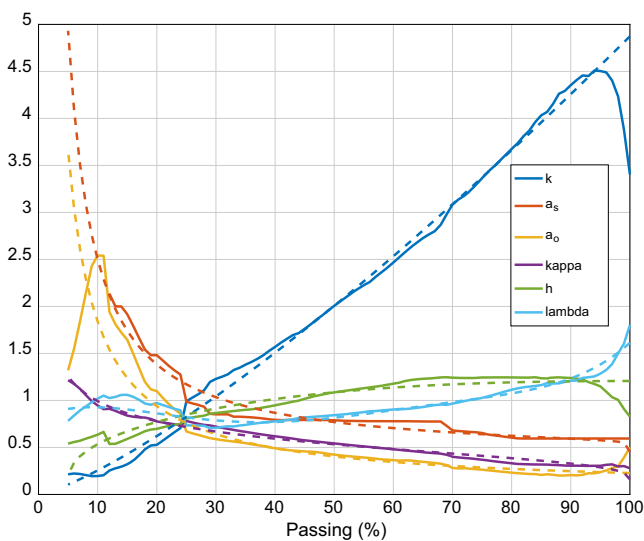


Fig. 7 Delay function (Eq. 43) for x_{50}

much narrower than the basic, four-parameter one in Fig. 4, with mean 0.0028, still slightly skewed with 95% coverage $[-0.064, 0.093]$. Figure 7 shows the delay function.

Many possible characteristic lengths L_c have been tested (burden, spacing, bench height, stemming length, charged length and geometric means of their pairs); the geometric mean of bench height and spacing has been observed to generally provide a best fit of the final model: $L_c = (H \cdot S)^{1/2}$. The shape factor k_2 from Eq. 16 is then:

$$k_2 = \frac{BHS}{(HS)^{3/2} \cos \theta} = \frac{B}{\sqrt{HS} \cos \theta} \tag{44}$$



The characteristic lengths for non-dimensionalizing the joints spacing and the delay have also been selected from tests with different lengths; the best fits are obtained with the burden for the joints spacing term and the holes spacing for the delay factor: $L_j = B, L_r = S$.

About the strength factor $\bar{\sigma}$, several rock properties have been tested, and the ratio $\sigma_c^2/(2E)$ —the elastic strain energy at rupture per unit volume—has finally been chosen as the one giving the most favorable fits to the data. This energy appears in Griffith’s (1921) energy balance of linear elastic fracture mechanics, in which the strain energy released by a crack equals the elastic strain energy.

5 Results and Discussion

The function in Eq. 42 with the delay function $f_r(\Pi_r)$ in Eq. 43 has been fitted to percentiles from 100 to 5. The parameters are plotted in Fig. 8 as functions of the percentage passing. Table 7 summarizes some quality figures of the fits. Note that the p values are very low for all parameters and all percentiles, which indicate very tight confidence intervals, an outstanding result for a nine-parameter model fit.

For ease of application of the model, approximating functional forms have been derived for the nine parameters as functions of P . The result is summarized in Table 8, and the P -functions are plotted in Fig. 8 as dashed lines. Note that not all the functions are direct fits to the parameters; functions for k, κ and the delay parameters are fitted first, and then, the model is adjusted again to the other parameters, for which analytic functions of P are finally obtained.

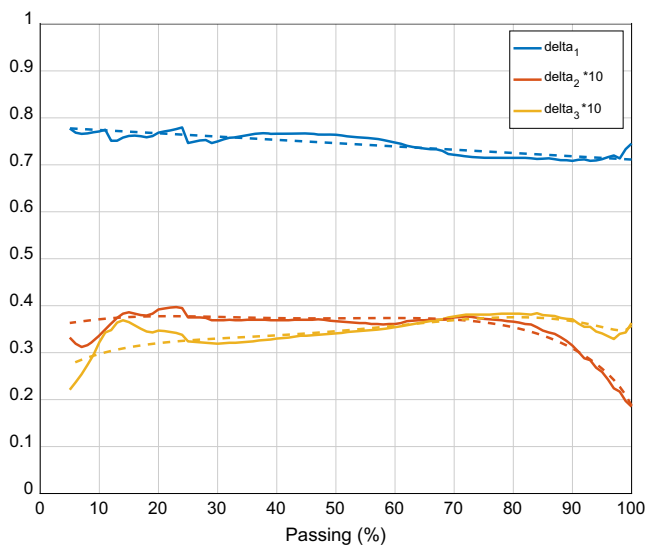


Fig. 8 Parameters of the model. *Left* k, a_s, a_o, κ, h and λ . *Right* parameters of the delay function. *Solid lines* model fit results; *dashed lines* approximated functions

Table 7 Quality values of the fits

P	Raw fits			p values										Functions in Table 8		
	R ²	RRMSE	MALE _r	k	a _s	a ₀	κ	h	λ	δ ₁	δ ₂	δ ₃	R ²	RRMSE	MALE _r	
100	0.8122	0.3582	0.2206	3.1E-05	3.7E-18	2.9E-03	9.9E-05	5.2E-14	2.3E-04	3.4E-34	2.4E-03	4.7E-03	0.7813	0.3749	0.2739	
95	0.8564	0.3401	0.1800	2.7E-07	7.9E-29	9.4E-03	2.1E-06	1.6E-26	3.4E-05	1.1E-38	2.3E-06	5.1E-06	0.8544	0.3395	0.1929	
90	0.8824	0.3279	0.1643	2.9E-08	3.2E-33	9.9E-03	3.7E-07	3.4E-32	1.3E-05	1.3E-43	5.7E-08	1.9E-08	0.8812	0.3339	0.1727	
80	0.9035	0.3172	0.1623	8.6E-09	3.3E-36	4.4E-03	1.1E-08	2.5E-34	2.5E-06	5.4E-47	3.8E-10	1.8E-11	0.9002	0.3352	0.1694	
70	0.9148	0.3115	0.1761	5.8E-09	1.4E-38	2.0E-03	2.7E-12	3.8E-36	3.9E-08	1.2E-48	2.7E-11	1.1E-12	0.9120	0.3246	0.1651	
60	0.9220	0.3039	0.1974	6.5E-09	7.8E-47	4.3E-04	5.4E-17	3.7E-35	1.9E-10	8.1E-48	7.3E-12	1.1E-12	0.9199	0.3089	0.1875	
50	0.9242	0.2992	0.1840	1.1E-08	1.6E-44	1.8E-04	3.1E-20	1.4E-31	1.6E-11	1.1E-46	1.3E-12	3.1E-13	0.9235	0.3022	0.1792	
40	0.9223	0.2983	0.1964	3.7E-08	3.8E-40	1.0E-04	1.4E-23	2.3E-25	4.0E-12	9.5E-45	3.8E-13	2.5E-13	0.9202	0.3020	0.2078	
30	0.9154	0.3298	0.2104	6.0E-07	3.2E-31	1.3E-04	1.4E-25	7.1E-20	1.0E-11	8.8E-41	1.0E-12	2.2E-12	0.9128	0.3325	0.2111	
20	0.9115	0.3827	0.2322	1.9E-04	6.5E-13	4.1E-04	1.1E-19	5.7E-13	5.5E-12	6.7E-35	1.0E-09	1.0E-09	0.9101	0.3801	0.2238	
10	0.9202	0.3654	0.1969	1.2E-06	0.0E+00	1.8E-06	1.5E-31	8.7E-13	4.7E-35	4.8E-35	1.6E-08	3.2E-08	0.9172	0.3653	0.1892	
5	0.9131	0.3998	0.2105	3.6E-06	0.0E+00	4.6E-05	1.8E-33	5.2E-09	3.1E-26	8.0E-22	9.0E-13	2.2E-11	0.8897	0.4693	0.2208	

R², determination coefficient; RRMSE, relative root-mean-squared error; MALE_r, median absolute logarithmic error, expressed as relative error

This two-step procedure allows to correct the errors from the fits in the first step, which otherwise might combine to give, in some cases, odd results. *k*, being P^r/k^i , has been chosen a monotonic function of *P* since the fragments shape factor is likely not to change much with *P*. In doing this, we assume that the observed decrease in *k* at high *P* is not a strong result (just as the mild increase below *P* = 10%) and is due to inaccuracies, always greater at high and low percentages passing. The functional form of $\kappa(P)$ is also assumed a priori, and it will be revisited below.

Figure 9 shows the resulting set of delay functions for the different percentages passing.

The overall goodness of the fits is assessed in Fig. 10 where boxplots of logarithmic errors (as defined in Eq. 34) are plotted for the calculations using both the raw parameters from the fits and the functions of Table 8. The penalty for using Table 8 formulae with respect to using the raw parameter values is small. The prediction error is 50% of the times less than about 25% in nearly the whole range both with the raw parameters and with their fitting functions. The boxplots in Fig. 10 are equivalent to those in Fig. 1 for the Kuz-Ram and crush zone models (in fact, log errors in Fig. 1 are also *w_e*-corrected, as in Eq. 34). The comparison of both is self-explanatory.

Another way of assessing the errors is in terms of the median (used for robustness) error of the size calculation for each data set, in absolute value; for $i = 1, \dots, n_c$, n_c being the number of data sets (169):

$$e_{Li} = \text{med}|e_{Lij}|, \quad j = 1, \dots, 20 \tag{54}$$

where e_{Lij} are log errors (as in Eq. 34) of the size at passing $P_j = 5, 10, \dots, 100$. The distribution of these errors, expressed as relative errors, $\exp(e_{Li}) - 1$, is given as boxplots in Fig. 11. This confirms an expected error of the percentile size prediction in the range of 20%. Plots are also shown for the Kuz-Ram and crush zone models, the median error of which (i.e., the expected error) is about 60%.

The 20–25% expected errors of the model should be viewed in the context of fragment size measurements. All data used were obtained by sieving and weighing samples of the muckpile—in many cases a large fraction of that, encompassing large amounts of material. Sampling, screen processing and weighing a large amount of rock fragments in field conditions is a hard task prone to errors. The sampling must be done on a significant fraction of the muckpile and from the different zones in it; loader sampling and dumping techniques, and end effects in the pile, are responsible for shifts in the size distributions (Stagg and Rholl 1987); the type of sieve (square, rectangular, grizzly, etc.) has an influence on the screening results; losses of material due to overweights (not loadable onto the screen), projections, fines, etc. also introduce errors.

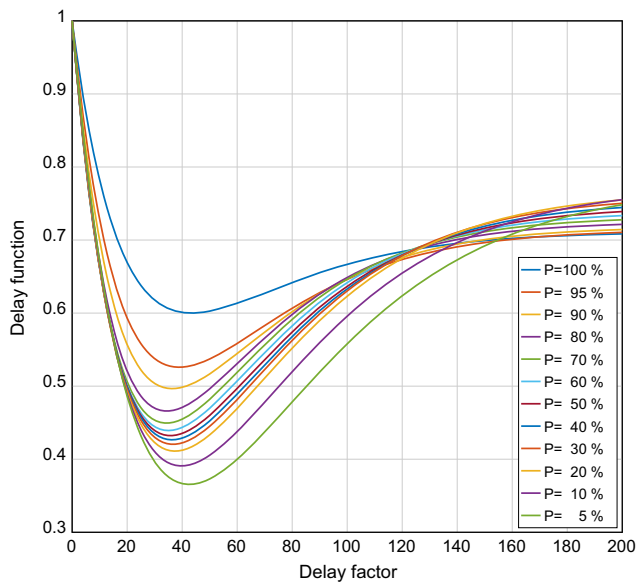


Fig. 9 Delay functions (Eq. 43, with coefficients from Eqs. 51–53)

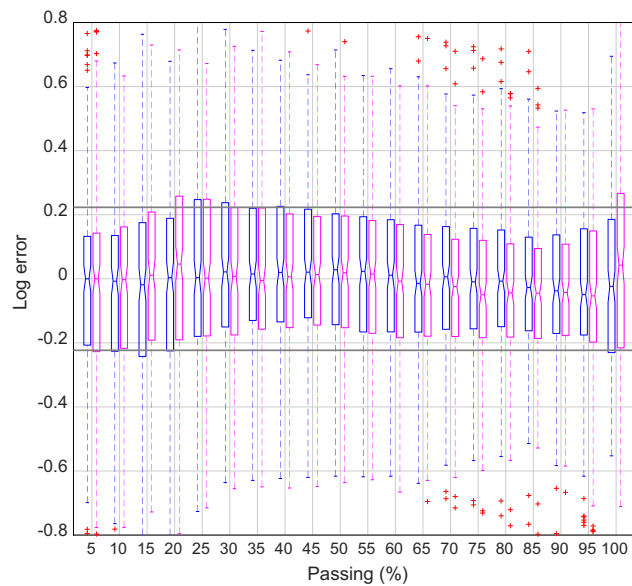


Fig. 10 Boxplots of logarithmic errors (Eq. 34) of the calculated percentiles. *Blue boxes* are the errors using the raw parameters, and *magenta boxes* are the errors using the functions in Table 8. The *gray horizontal lines* are plotted at $\pm \ln 1.25$, equivalent to relative errors of 25% (color figure online)

Since the data come from different sources, a general statement on the error of the data is difficult to give, nor is it usually assessed by the authors. Sanchidrián (2015) estimated the uncertainty of the data by calculating the differences of equal percentile sizes of pairs of similar blasts (i.e., blasts in the same mine or quarry with equal, or very close, blast design¹³) for which fragmentation should be (ideally) the same; such differences are a combined measure of the uncertainty of the fragmentation

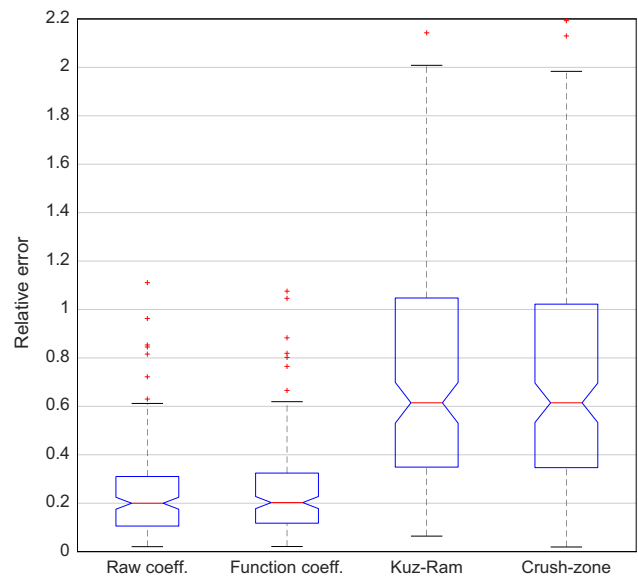


Fig. 11 Distributions of the medians of the absolute errors for all percentiles for each data set (Eq. 54, transformed to relative errors)

measurement (due to sampling, sieving and weighing), the variability of the phenomenon and the uncertainty of the blasting data. To all those, the calculation of sizes at some given percentages passing adds an interpolation error. The median differences for percentiles 5–100 was found to be between 8 and 22%. Even if this is only a rough estimation of the uncertainty, and does not include possible systematic measurement errors, it gives an idea of how much accuracy we should be prepared to demand from a fragmentation prediction model, as there is no way we can have a better knowledge of the actual fragmentation than what the measurements give us.

Figure 12 shows some sample size distribution curves calculated, compared with the data; the P -functions for the model parameters are used. Each graph shows distributions for which the relative errors are around the first quartile, the median and the third quartile, plus one more in which the three best and the three worst predicted distributions, as from the median absolute value of the log error, are plotted.

One of the ideas that inspired this fragment size distribution model in which the exponent of the powder factor is

¹³ The concept ‘equal blast design’ is itself somewhat ambiguous since it is often difficult to determine the blasting parameters exactly; for instance, the powder factor, unless an extremely careful explosive mass and dimensional monitoring of the blasted rock is implemented, can have a certain variation for two seemingly identical blasts due to small variations of the blast hole diameter (bit wear), the bench height and burden, or the explosive density; delay time with pyrotechnic delay systems is also an undetermined variable; minor variations in the rock properties from one blast to another also make up for uncertainty in the fragmentation, etc.

Table 8 Functional forms of the parameters; P is fraction passing, $0.05 \leq P \leq 1$

$k = 4.873P^{1.280}$	(45)	$R^2 = 0.9993$ (R); RRMSE = 0.0169
$a_s = 0.4539 + 0.1557P^{-1.123}(1 - P)^{0.1}$	(46)	$R^2 = 0.9873$ (R); RRMSE = 0.0389
$a_o = 0.05431 + 0.1737P^{-1.012}$	(47)	$R^2 = 0.9949$ (O); RRMSE = 0.0707
$\kappa = 0.161 + 0.373\left(\frac{1}{P} - 1\right)^{0.3648}$	(48)	$R^2 = 0.9772$ (O); RRMSE = 0.0610
$h = 1.207(P - 0.04744)^{0.3152(1-P)^{1.25}}$	(49)	$R^2 = 0.9683$ (O); RRMSE = 0.0417
$\lambda = 0.8201 + 2.773P - 22.33P^2 + 59.62P^3 - 65.06P^4 + 25.79P^5$	(50)	$R^2 = 0.9335$ (O); RRMSE = 0.0564
$\delta_1 = 0.7811 - 0.06989P$	(51)	$R^2 = 0.7337$ (O); RRMSE = 0.0158
$\delta_2\delta_3 = 0.000836 + 0.003832P - 0.0137P^2 + 0.0217P^3 - 0.012P^4$	(52)	$R^2 = 0.7528$ (O); RRMSE = 0.0776
$\frac{\delta_2}{\delta_3} = P^{-0.09161}(1.01 - P)^{0.2062}\exp(0.3034P)$	(53)	$R^2 = 0.9733$ (R); RRMSE = 0.0237

R^2 , determination coefficient; RRMSE, relative root-mean-squared error (R) and (O) indicate robust and ordinary least squares fit, respectively

variable with P was the ‘fan’ pattern we referred to in Sect. 1 (Ouchterlony et al. 2016). If extrapolated toward very low (away from the feasible range) powder factor, the different percentile lines often converge (more or less precisely) in a focal point. The data used for the fits happen to meet that ‘fan’ pattern more than well (see the upper graphs of Fig. 13; the energy concentration is used instead of the charge concentration used in Fig. 2). Even if the dispersion is very large (due to the great variation of scale, rock and shape factors, and delay), the coefficients of the fits (shown on the right plot) are significant, their p values below 10^{-23} for the pre-factor and 0.03 for the exponent. The predicted results from the model also catch much of this behavior (Fig. 13, lower graphs; the P -functions for the parameters have been used for the calculation); the p values of the coefficients (shown in the right plot) are less than 10^{-22} for the pre-factor and 0.02 for the exponent. As an exercise to confirm this, without any cross-influence, a sample calculation with constant blast characteristics (Table 9) and with the powder factor only variable (implemented by varying the hole diameter) has been done; the results are shown in Fig. 14 for three delay times; the fanlike convergence is clearly visible.

The functional form of $\kappa(P)$ (Table 8, Eq. 48) has been taken from the expression derived by Ouchterlony et al. (2016) for the exponent of the size versus powder factor power equations—i.e., the log–log slope of the fan-plot lines—following the hypothesis that the underlying distribution is a Swebrec function (Ouchterlony 2005a, b, 2009a) with shape parameter independent of the powder factor. The determination coefficient of the fit of Eq. 48 to the P - κ values of the model is 0.9772. This result provides an interesting link of the model presented here with the powder factor fan plots and the Swebrec distribution.

It is worth noting that the detonation velocity of the explosive is not among the variables of the model. The

influence of detonation velocity in fragmentation is controversial: It appears only in the Kou and Rustan (1993) and Rustan and Nie (1987) formulae and is used in the crush zone model for the calculation of the borehole pressure; conversely, it is not present in the Kuz-Ram model (Cunningham 1983, 1987, 2005) and other fragmentation prediction formulae (Langefors and Kihlström 1963; Holmberg 1974; Larsson 1974; Chung and Katsabanis 2000).

In the present model, detonation velocity might influence the loading rate and the borehole pressure, both of which should in principle be relevant to fragmentation. Concerning the loading rate, the detonation velocity appears not to be the leading influence, since it varies in a relatively narrow range for most explosives used in rock blasting, while the reaction zone thickness appears to be much more important, as it varies in several orders of magnitude depending on the physical constitution and the sensitivity of the explosive. This is why explosives with not too different detonation velocity as, e.g., a straight emulsion and an emulsion/ANFO mixture have very different loading rates, as noted in Sect. 2.

About the borehole pressure, Boudet et al. (1996) gave the following expression of crack speed as function of the applied stress:

$$v_c/c_R = b\sqrt{1 - \frac{\Delta_1}{\Delta}} \quad (55)$$

where v_c is crack speed, c_R is Rayleigh wave speed and Δ strain, $\Delta = P_b/E$; b and Δ_1 are experimental constants, $b < 1$. The borehole pressure can be estimated, for a coupled explosive, as half of the detonation pressure, which can be approximated from the explosive density and detonation velocity squared. Thus, a non-dimensional delay factor to more correctly account for the time of arrival of the cracks to the proximity of the next hole in the firing sequence would be:

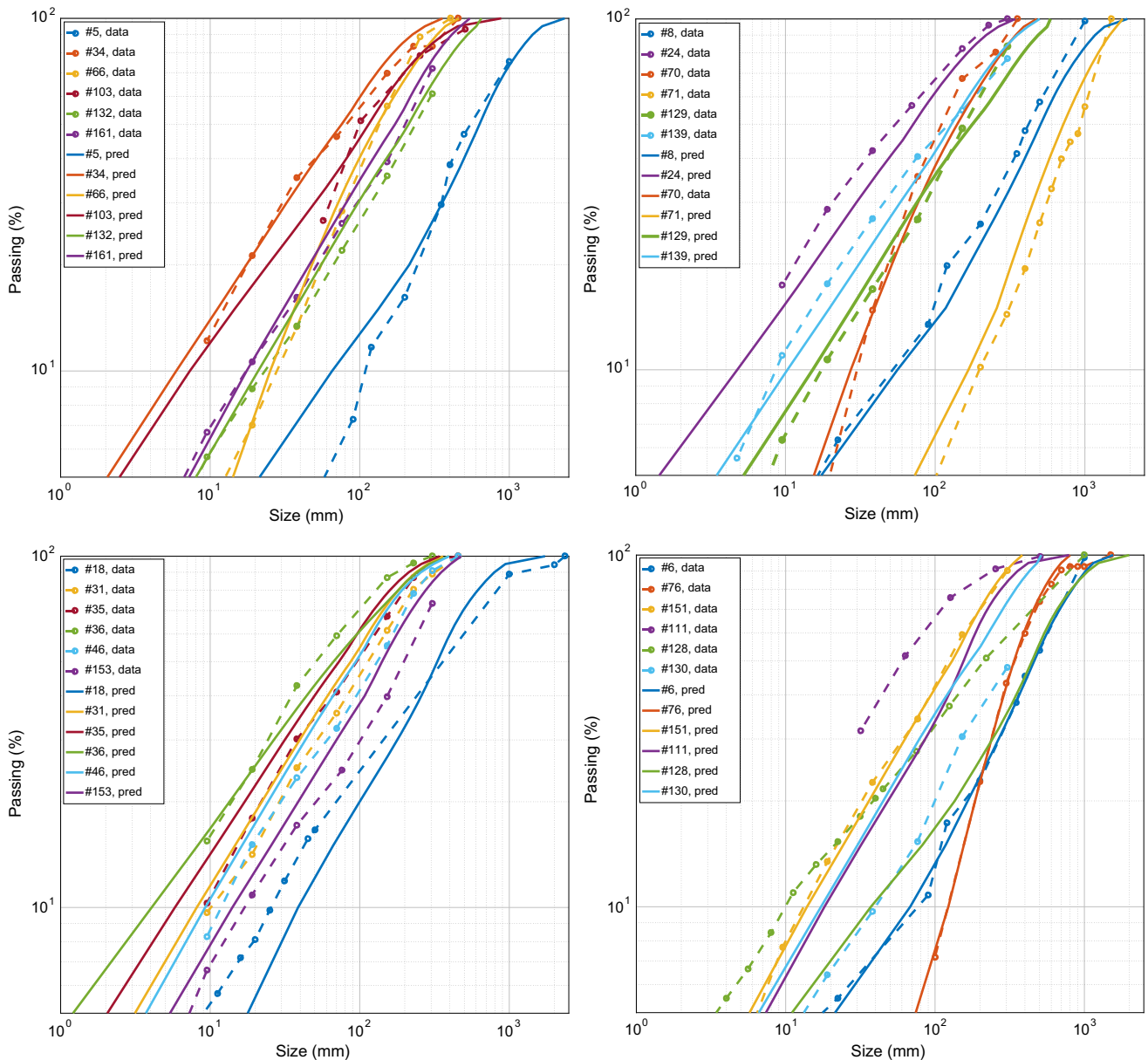


Fig. 12 Sample size distribution curves; *dashed* data, *solid* calculated. Median relative error of the curves plotted: *upper left* 11.0–12.6% (around the first quartile); *upper right* 19.4–21.0%

(around the median); *lower left* 30.5–33.1% (around the third quartile); *lower right* 2.1–3.4% (the three best results), 88.3–107.6% (the three worst results)

$$\Pi_t = \frac{c_R \Delta t}{L_t} \sqrt{1 - \frac{\Delta_1}{\rho_e D^2 / E}} \quad (56)$$

where Δ_1 , an unknown property of the rock, must, however, be left as a parameter of the fit. As pointed out in Sect. 4, the wave velocity reported in our data is the P-wave one, so that, in order to use Eq. 56, we must successively estimate the shear wave and the Rayleigh wave velocities. Tests with this delay factor were not satisfactory, perhaps due to the lack of precision of the Rayleigh wave velocity estimation or to the constant Δ_1 assumption.

A similar form to Eq. 56 but using directly the P-wave velocity instead of the Rayleigh wave one also failed. In summary, we have not been able to account for the two explosive/rock interaction processes on which detonation velocity could be influential. Perhaps better data, with a more detailed description of the detonation physics and the rock velocities, are required.

Other parameters that are not part of the model are:

- *Number of rows* Some of the variability in the data is probably due to this factor. Blasts used to fit the model were single and multi-row (see Table 5), with 3 or 4

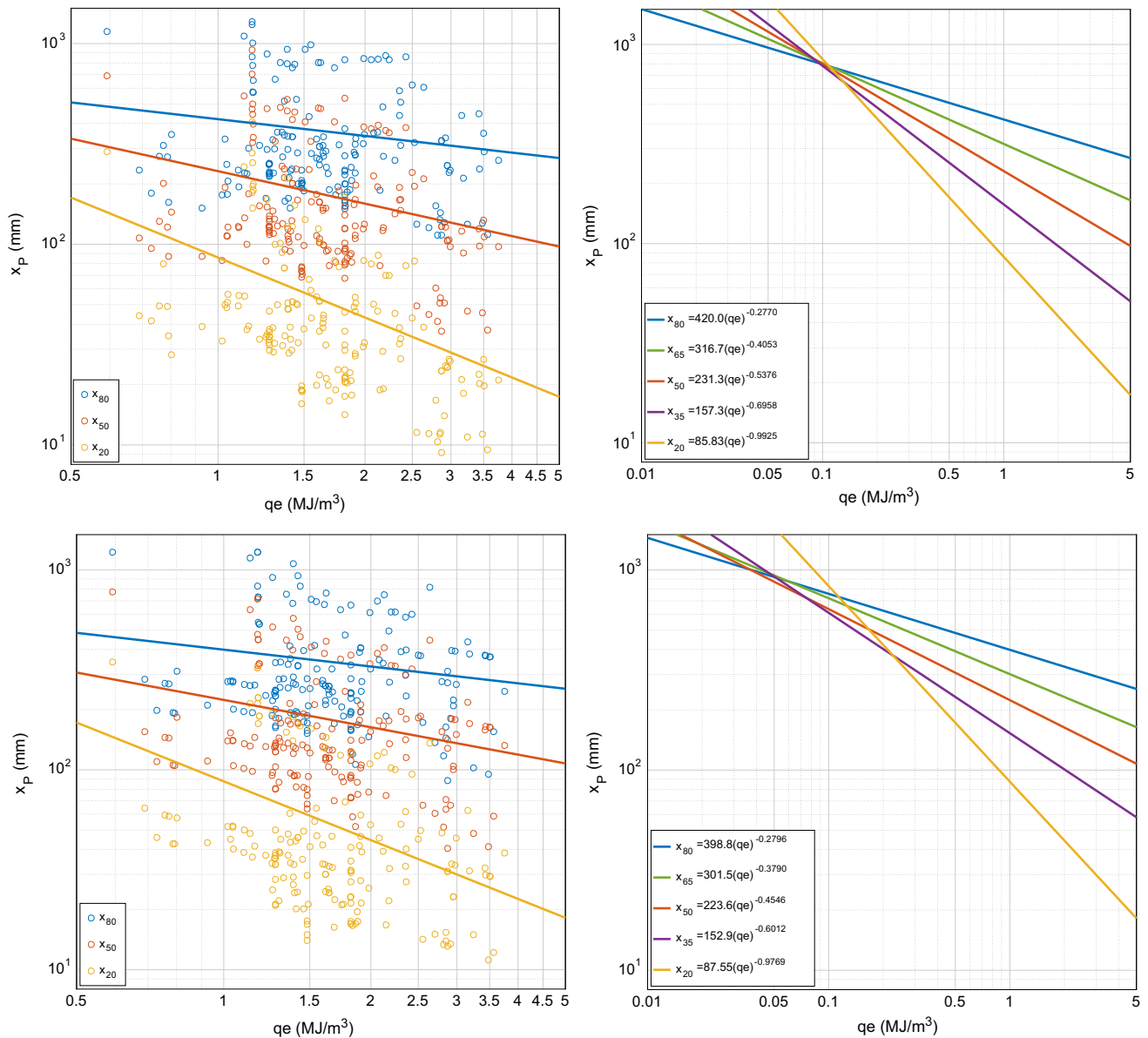


Fig. 13 ‘Fan plots’ of percentile sizes versus energy powder factor. *Upper graphs* data. *Lower graphs* predicted values. The *right graphs* show the extrapolation of the percentile power lines toward lower energy factors

rows and inter-row delays ranging from 24 to 120 ms, that correspond from 12 to 61 ms/m burden. Schimek et al. (2015) and Ivanova et al. (2015) reported the median size finer for the second and third rows of holes than for the first row, in tests with small-scale bench-like specimens (210 mm height, 70×95 mm burden \times spacing, seven holes per row), where the first row was blasted in virgin material. This is seldom the case in mining or quarrying where, even if only one row is blasted, the burden has usually been damaged by the previous blasts in front of it. Error distributions for blasts with one and several rows have been compared by the Wilcoxon–Mann–Whitney test, and they are not different at a 0.05 significance in the range 40–95%

passing, but they are below 40% and also at the maximum size. Attempts to incorporate the number of rows into a significant term yielding an improved predictive capability to the model have been unsuccessful. Two major difficulties have been encountered for it: (1) the amount of data for multi-row blasts is significantly smaller than the one row: only 35 blasts out of 169 are multiple row, and, more importantly, (2) there is a significant cross-correlation between the number of rows and the size of the blast in the data used. The results were in all cases a loss of significance (high p value) of some of the parameters of the model, or a marginal gain in the determination coefficient, or both. Be that as it may, the influence of both the

Table 9 Blast data for sample calculation

Rock	
Discontinuity spacing	$s_j = 0.5$ m
Discontinuity orientation	Dipping toward face, $j_o = 0.5$
Uniaxial compressive strength (MPa)	$\sigma_c = 100$ MPa
Elastic modulus	$E = 25$ GPa
P-wave velocity	$c_p = 4000$ m/s
Geometry	
Bench height	$H = 10$ m
Burden	$B = 3.0$ m
Spacing	$S = 3.2$ m
Holes inclination	0
Stemming length	$l_s = 2.5$ m
Subdrill length	$l_j = 1.0$ m
Hole diameter	50–150 mm
Explosive	
Explosive energy	$e = 3.5$ MJ/kg
Explosive density	$\rho_e = 1200$ kg/m ³
In-row delay	$\Delta t = 0, 10, 30$ ms
Powder factor, mass	$q = 0.21\text{--}1.88$ kg/m ³
Powder factor, energy	$qe = 0.73\text{--}6.57$ MJ/m ³

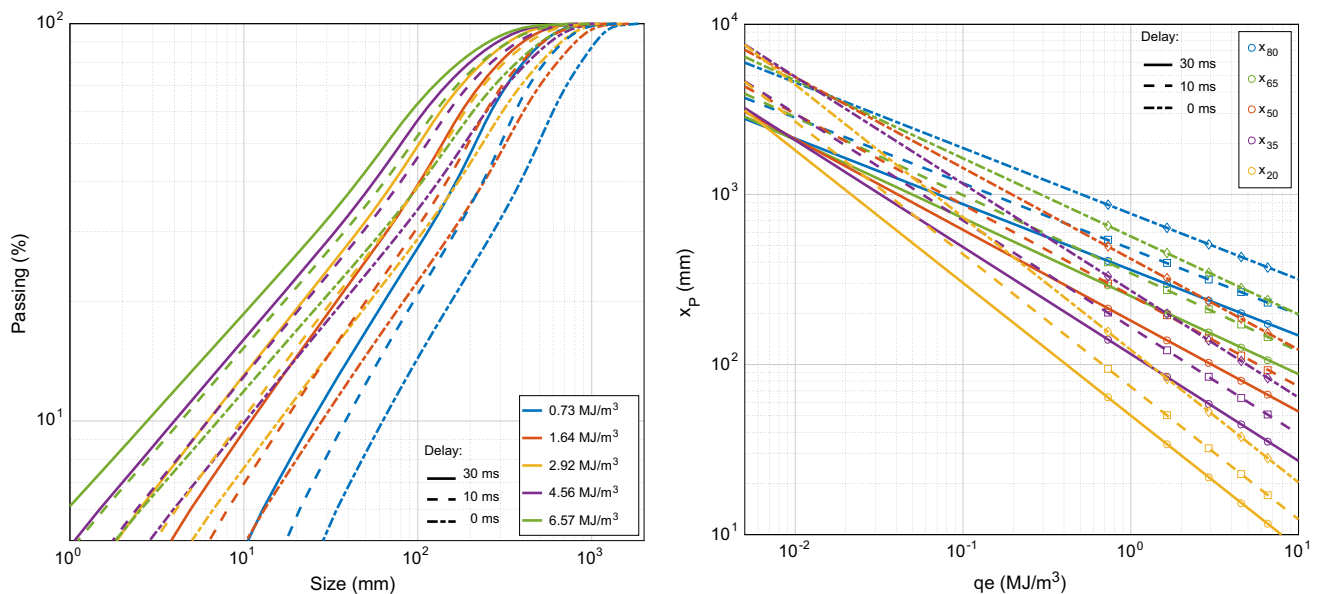


Fig. 14 Sample fragmentation calculation. *Left* size distributions; *right* percentiles versus powder factor fan plots. In-row delay 30 ms (solid lines), 10 ms (dashed lines) and zero (dash-dotted lines)

number of rows and the row-to-row relief time remain a subject of further study.

- *Detonator precision* The amount of blasts with precise initiation (so considered if the time error is less than 1 ms) and non-precise initiation is fairly balanced: 78 precise (seismic, electronic and exploding bridge wire detonators) and 91 non-precise (pyrotechnic, both electric and non-electric). The error analysis for the two precision categories shows no difference in the error distributions

for precise and non-precise initiated blasts in the whole 100–5 percentile range at a 0.05 significance.

6 Conclusions

A model for fragmentation by blasting has been built taking as starting point asteroid collisional fragmentation theory from which non-dimensional functional forms of the

percentile sizes of the fragments distribution are derived. These functions include a scaling length and two non-dimensional factors: a rock strength-to-energy concentration ratio and a bench shape factor. The model is calibrated with data from 169 blasts for which the blast design variables were reported and the muckpile was sampled and sieved to determine the size distribution. Two additional factors are found to be required: one of them to account for the rock structure—the joints spacing and orientation—and the other for the delay between holes.

The scaling of the percentile sizes has been found to be optimum using the geometric mean of the bench height H and the spacing S . The bench shape factor is the ratio of the nominal volume excavated by a blasthole to the scaling length cubed.

The rock strength-to-explosive energy factor is the ratio of the resistance capacity (the strength) of the rock to the driving explosive force; the rock strength is described by the strain energy at rupture per unit volume $\sigma_c^2/(2E)$, σ_c being the uniaxial compressive strength and E the Young's modulus. The selection of this parameter has been done on a purely numerical screening of strength variables giving the best determination of the final model. The explosive yield is described as the energy concentration per unit volume, in a direct transpose of the asteroid collision that uses the impactor kinetic energy. Energy concentration is calculated as the powder factor times the explosive energy per unit mass; the explosive energy is rated with the common heat of explosion value.

The rock structure is accounted by a linear form of the joints spacing and the joint orientation descriptions. The joints spacing is written using its non-dimensional ratio to the burden. The joints orientation term is Lilly's number normalized to one.

The influence of the delay is found to be a function of the non-dimensional factor $c_P \Delta t / S$; the function decreases as the delay factor increases, reaching a minimum at a certain value of the factor (in the range 30–40 for most percentiles), beyond which the function increases toward an asymptotic value.

The model is applied from 5 to 100 percentile sizes. All the parameters of the model have tight confidence intervals, which indicate a well-conditioned function and a robust model of the existing data with good predictive capability. The expected prediction error is about 20% across the 100–5 percentile range.

Acknowledgements The authors are really grateful to Prof. Norbert H Maerz, Missouri University of Science and Technology at Rolla, MO, for 'excavating' a large number (42) of our fragmentation data sets from early blasting tests with sieving at Rolla and putting them at our disposal. They would also like to thank Prof. Peter Moser, Montanuniversitaet Leoben, for his long-term enthusiastic support of fragmentation by blasting research and his long-standing friendship.

Funding Funding was provided by Universidad Politécnica de Madrid and MONTANUNIVERSITAET LEOBEN.

Open Access This article is distributed under the terms of the Creative Commons Attribution 4.0 International License (<http://creativecommons.org/licenses/by/4.0/>), which permits unrestricted use, distribution, and reproduction in any medium, provided you give appropriate credit to the original author(s) and the source, provide a link to the Creative Commons license, and indicate if changes were made.

References

- Adebola JM, Ajayi OD, Elijah P (2016) Rock fragmentation prediction using Kuz-Ram model. *J Environ Earth Sci* 6(5):110–115
- Ash RL (1973) The influence of geological discontinuities on rock blasting. Ph.D. thesis, University of Minnesota, Minneapolis
- Baron LI, Sirotyuk GN (1967) Verification of the applicability of the Rozin–Rammler equation for calculation of the mean diameter of a fragment with the explosive breaking of rock. *Explosive Engineering* no. 62/19, Izd Nedra, Moscow (in Russian)
- Bekkers G (2009) A practical approach to fragmentation optimization at Kidd Mine. In: Sanchidrián JA (ed) Proceedings of 9th international symposium on rock fragmentation by blasting (Fragblast 9), Granada, Spain, 13–17 September 2009. CRC Press/Balkema, Leiden, pp 761–768
- Bergmann OR, Wu FC, Edl JW (1974) Model rock blasting measures effect of delays and hole patterns on rock fragmentation. *E/MJ Mining Guidebook: Systems for Emerging Technology*, June, pp 124–127
- Bleakney EE (1984) A study on fragmentation and ground vibration with air space in the blasthole. M.Sc. Thesis, University of Missouri-Rolla
- Borquez GV (2006) Drilling, blasting, primary crusher productivity—a macro-system view of fragmentation to efficiently recover mineral resources. Proceedings of 8th international symposium on rock fragmentation by blasting (Fragblast 8), Santiago, Chile, 7–11 May 2006. Editec, Santiago, pp 240–245
- Boudet J, Ciliberto S, Steinberg V (1996) Dynamics of crack propagation in brittle materials. *J Phys II* 6(10):1493–1516
- Brinkmann JR (1982) The influence of explosive primer location on fragmentation and ground vibrations for bench blasts in dolomitic rock. M.Sc. Thesis, University of Missouri-Rolla
- Brunton I, Jankovic A, Kanchibotla S, Licina T, Thornton D, Valery W (2001) Mine to mill optimisation at Porgera gold mine. JKMR internal report
- Cáceres Saavedra J, Katsabanis PD, Pelley CW, Kelebek S (2006) A neural network model for fragmentation by blasting. Proceedings of 8th international symposium on rock fragmentation by blasting (Fragblast 8), Santiago, Chile, 7–11 May 2006. Editec, Santiago, pp 200–206
- Chung SH, Katsabanis PD (2000) Fragmentation prediction using improved engineering formulae. *Fragblast Int J Blasting Fragm* 4(3–4):198–207
- Cunningham CVB (1983) The Kuz-Ram model for prediction of fragmentation from blasting. In: Holmberg R, Rustan A (eds) Proceedings of 1st international symposium on rock fragmentation by blasting, Luleå, Sweden, 22–26 August 1983. Luleå Tekniska Universitet, Luleå, pp 439–453
- Cunningham CVB (1987) Fragmentation estimations and the Kuz-Ram model—four years on. In: Fournery WL, Dick RD (eds) Proceedings of 2nd international symposium on rock fragmentation by blasting, Keystone, CO, 23–26 August 1987. Society of Experimental Mechanics, Bethel, pp 475–487

- Cunningham CVB (2005) The Kuz-Ram fragmentation model—20 years on. In: Proceedings of 3rd world conference on explosives and blasting, Brighton, UK, 13–16 September 2005, pp 201–210
- Daehnke A, Rossmann HP, Knasmillner RE (1996) Blast-induced dynamic fracture propagation. In: Mohanty B (ed) Proceedings of 5th international symposium on rock fragmentation by blasting (Fragblast 5), Montreal, Canada, 25–29 August 1996. Balkema, Rotterdam, pp 13–18
- Dick RA, Fletcher LR, D'Andrea DV (1973) A study of fragmentation from bench blasting in limestone at a reduced scale. USBM report of investigation RI 7704, US Bureau of Mines
- Djordjevic N (1999) Two-component model of blast fragmentation. In: Proceedings of 6th international symposium on rock fragmentation by blasting (Fragblast 6), Johannesburg, South Africa, 8–12 August 1999. Symposium series S21. SAIMM, Johannesburg, pp 213–219
- Dulaney EP, Brace WF (1960) Velocity behavior of a growing crack. *J Appl Phys* 31:2233–2236
- Eissa EA, Kazi A (1988) Relation between static and dynamic Young's moduli for rocks. *Int J Rock Mech Min* 25:479–482
- Engin IC (2009) A practical method of bench blasting design for desired fragmentation based on digital image processing technique and Kuz-Ram model. In: Sanchidrián JA (ed) Proceedings 9th international symposium on rock fragmentation by blasting (Fragblast 9), Granada, Spain, 13–17 September 2009. CRC Press/Balkema, Leiden, pp 257–263
- Faramarzi F, Ebrahimi Farsangi MA, Mansouri H (2015) Prediction of rock fragmentation using gamma-based blast fragmentation distribution model. In: Spathis AT et al (eds) Proceedings of 11th international symposium on rock fragmentation by blasting (Fragblast 11), Sydney, Australia, 24–26 August 2015. The Australasian Institute of Mining and Metallurgy, Carlton, pp 685–692
- Ford RM (1997) A model for minimizing the cost of rock mass excavation. M.Sc. Thesis, University of Arizona
- Fourney WL (2015) The role of stress waves and fracture mechanics in fragmentation. *Blasting Fragm* 9(2):83–106
- Freund LB (1972) Crack propagation in an elastic solid subjected to general loading. *J Mech Phys Solids* 20:129–152
- Gates AO (1915) Kick vs. Rittinger: an experimental investigation in rock crushing performed at Purdue University. *Trans AIME* 52:875–909
- Gaudin AM (1926) An investigation of crushing phenomena. *Trans AIME* 73:253–316
- Gheibie S, Aghababaei H, Hoseinie SH, Pourrahimian Y (2009a) Kuznetsov model's efficiency in estimation of mean fragment size at the Sungun copper mine. In: Sanchidrián JA (ed) Proceedings of 9th international symposium on rock fragmentation by blasting (Fragblast 9), Granada, Spain, 13–17 September 2009. CRC Press/Balkema, Leiden, pp 265–269
- Gheibie S, Aghababaei H, Hoseinie SH, Pourrahimian Y (2009b) Modified Kuz—Ram fragmentation model and its use at the Sungun Copper Mine. *Int J Rock Mech Min* 46(6):967–973
- Griffith AA (1921) The phenomena of rupture and flow in solids. *Phil Trans R Soc Lond A* 221:163–198
- Gynnemo M (1997) Investigation of governing factors in bench blasting. Full-scale tests at Källered and Billingsryd. Publ A84, Chalmers University, Department of Geology, Gothenburg, Sweden (In Swedish)
- Hafsaoui A, Talhi K (2009) Influence of joint direction and position of explosive charge on fragmentation. *Arab J Sci Eng* 34(2A):125–132
- Hirosaki Y, Murata K, Kato Y, Itoh S (2002) Effect of void size on the detonation pressure of emulsion explosives. In: Furnish MD, Thadhani NN, Horie Y (eds) Shock Compression of condensed matter—2001. American Institute of Physics, College Park, pp 930–933
- Hoek E, Brown ET (1980) Underground excavations in rock. Institute of Mining and Metallurgy, London, pp 155–156
- Holmberg R (1974) Charge calculations for bench blasting. SveDeFo Report DS 1974:4, Swedish Detonic Research Foundation, Stockholm (In Swedish)
- Holsapple KA, Schmidt RM (1987) Point source solutions and coupling parameters in cratering mechanics. *J Geophys Res* 92(B7):6350–6376
- Housen KR, Holsapple KA (1990) On the fragmentation of asteroids and planetary satellites. *Icarus* 84:226–253
- Ivanova R, Ouchterlony F, Moser P (2015) Influence of distorted blasthole patterns on fragmentation as well as roughness of, and blast damage behind, remaining bench face in model-scale blasting. In: Spathis AT et al (eds) Proceedings of 11th international symposium on rock fragmentation by blasting (Fragblast 11), Sydney, Australia, 24–26 August 2015. The Australasian Institute of Mining and Metallurgy, Carlton, pp 693–705
- Jaeger JC, Cook NGW (1969) Fundamentals of rock mechanics. Methuen, London, p 184
- Jahani M, Taji M (2015) Comparison of empirical fragmentation models at the Gol—Gohar iron ore mine. In: Spathis AT et al (eds) Proceedings of 11th international symposium on rock fragmentation by blasting (Fragblast 11), Sydney, Australia, 24–26 August 2015. The Australasian Institute of Mining and Metallurgy, Carlton, pp 707–713
- Johansson D, Ouchterlony F (2013) Shock wave interactions in rock blasting—the use of short delays to improve fragmentation in model-scale. *Rock Mech Rock Eng* 46(1):1–18
- Kanchibotla SS, Valery W, Morrell S (1999) Modelling fines in blast fragmentation and its impact on crushing and grinding. Proceedings of Explo'99—a conference on rock breaking, Kalgoorlie, WA, 7–11 November 1999. The Australasian Institute of Mining and Metallurgy, Carlton, pp 137–144
- Katsabanis PD, Liu L (1996) Delay Requirements for fragmentation optimization. In: Franklin JA, Katsabanis T (eds) Measurement of Blast Fragmentation. Balkema, Rotterdam, pp 241–246
- Katsabanis PD, Omidi O (2015) The effect of the delay time on fragmentation distribution through small- and medium-scale testing and analysis. In: Spathis AT et al (eds) Proceedings of 11th international symposium on rock fragmentation by blasting (Fragblast 11), Sydney, Australia 24–26 August 2015. The Australasian Institute of Mining and Metallurgy, Carlton, pp 715–720
- Katsabanis PD, Tawadrous A, Braun A, Kennedy C (2006) Timing effects on the fragmentation of small blocks of granodiorite. *Fragblast Int J Blasting Fragm* 10(1–2):83–93
- Katsabanis P, Omidi O, Rielo O, Ross P (2014) A review of timing requirements for optimization of fragmentation. Proceedings of 40th annual conference on explosives and blasting technique, Denver, CO, 9–12 February 2014. The International Society of Explosives Engineers, Cleveland, pp 547–558
- Kojovic T, Michaux S, McKenzie C (1995) Impact of blast fragmentation on crushing and screening operations in quarrying. Proc Explo'95—a conference exploring the role of breakage in mining and quarrying, Brisbane, Australia, 4–7 September 1995. The Australasian Institute of Mining and Metallurgy, Carlton, pp 427–436
- Koshelev EA, Kuznetsov VM, Sofronov ST, Chernikov AG (1971) Statistics of fragments formed when solids are crushed by blasting. *Zh Prikl Mekh Tekh Fiz* 2:87–100 (in Russian)
- Kou S, Rustan A (1993) Computerized design and result predictions of bench blasting. In: Rossmann HP (ed) Proceedings of 4th international symposium on rock fragmentation by blasting

- (Fragblast 4), Vienna, Austria, 5–8 July 1993. Balkema, Rotterdam, pp 263–271
- Kuznetsov VM (1973) The mean diameter of the fragments formed by blasting rock. *Soviet Mining Sci* 9:144–148
- Langefors U, Kihlström B (1963) The modern technique of rock blasting. *Almqvist & Wicksell*, Uppsala
- Larsson B (1974) Report on blasting of high and low benches—fragmentation from production blasts. In: *Proceedings of discussion meeting BK74*, Swedish Rock Construction Committee, Stockholm, pp 247–273 **(In Swedish)**
- LeJuge GE, Cox N (1995) The impact of explosive performance on quarry fragmentation. *Proc Explo'95—a conference exploring the role of breakage in mining and quarrying*, Brisbane, Australia, 4–7 September 1995. The Australasian Institute of Mining and Metallurgy, Carlton, pp 445–452
- Lilly PA (1986) An empirical method of assessing rock mass blastability. In: Davidson JR (ed) *Proceedings of large open pit mine conference*, Newman, WA, October 1986. The Australasian Institute of Mining and Metallurgy, Parkville, pp 89–92
- Lilly PA (1992) The use of blastability index in the design of blasts for open pit mines. In: Szwedzicki T, Baird GR, Little TN (eds) *Proceedings of Western Australian conference on mining geomechanics*, Kalgoorlie, West Australia, 8–9 June 1992. Western Australia School of Mines, Kalgoorlie, pp 421–426
- Liu Q (2006) Modification of the Kuz-Ram model for underground hard rock mines. *Proceedings of 8th international symposium on rock fragmentation by blasting (Fragblast 8)*, Santiago, Chile, 7–11 May 2006. Editec, Santiago, pp 185–192
- Liu H, Lindqvist PA, Akesson U, Kou SQ, Lindqvist JE (2011) Characterisation of rock properties using texture-based modelling—a geometallurgical approach. In: *Proceedings of conference mineral engineering*, Luleå, 8–9 Feb 2011, Luleå Tekniska Universitet, Luleå
- Lownds CM (1983) Computer modelling of fragmentation from an array of shotholes. In: Holmberg R, Rustan A (eds) *Proceedings of 1st international symposium on rock fragmentation by blasting*, Luleå, Sweden, 22–26 August 1983. Luleå Tekniska Universitet, Luleå, pp 455–468
- Ma B, Zeng S, Zou D, Guo C (1983) A study of bench blasting in rhyolophyry at a reduced scale and the statistical analysis of the regularity for fragmentation distribution. In: Holmberg R, Rustan A (eds) *Proceedings of 1st international symposium on rock fragmentation by blasting*, Luleå, Sweden, 22–26 August 1983. Luleå Tekniska Universitet, Luleå, pp 857–872
- Marchenko LN (1965) Increase of the explosion efficiency in mining of minerals. *Nauka*, Moscow **(in Russian)**
- MATLAB Release 2015a (2015) The MathWorks, Inc., Natick
- McKenzie CK (2012) Limits blast design: Controlling vibration, gas pressure & fragmentation. In: Singh PK, Sinha A (eds) *Proceedings of 10th international symposium on rock fragmentation by blasting (Fragblast 10)*, New Delhi, India, 26–29 November 2012. CRC Press/Balkema, Leiden, pp 85–94
- Mitrovic SS, Kricak LM, Negovanovic MN, Jankovic IV, Zekovic DI (2009) Influence of rock mass blastability on explosive energy distribution. In: Sanchidrián JA (ed) *Proceedings of 9th international symposium on rock fragmentation by blasting (Fragblast 9)*, Granada, Spain, 13–17 September 2009. CRC Press/Balkema, Leiden, pp 249–255
- Morin MA, Ficarazzo F (2006) Monte Carlo simulation as a tool to predict blasting fragmentation based on the Kuz-Ram model. *Comput Geosci* 32(3):352–359
- Moser P, Grasedieck A, Olsson M, Ouchterlony F (2003) Comparison of the blast fragmentation from lab-scale and full-scale test at Bårarp. In: Holmberg R (ed) *Proceedings of EFEE 2nd world conference on explosives and blasting technique*, Prague, 10–12 September 2003, pp 449–458
- Olsson M, Bergqvist I (2002) Fragmentation in quarries. In: *Proceedings of discussion meeting BK 2002*. Swedish Rock Construction Committee, Stockholm, pp 33–38 **(in Swedish)**
- Ouederra I, Cavanaugh G, Torrance A (2011) Detonation pressure and temperature measurements of conventional and low-density explosives. *Proceedings Explo 2011—blasting-controlled productivity*, Melbourne, Australia, 8–9 November 2011. The Australasian Institute of Mining and Metallurgy, Carlton, pp 133–136
- Otterness RE, Stagg MS, Rholl SA, Smith NS (1991) Correlation of shot design parameters to fragmentation. *Proceedings of 7th symposium on explosives and blasting research*, Las Vegas, Nevada, 6–7 February 1991. Society of Explosives Engineers, Solon, pp 179–190
- Ouchterlony F (2005a) The Swebrec© function, linking fragmentation by blasting and crushing. *T I Min Metall A* 114:A29–A44
- Ouchterlony F (2005b) What does the fragment size distribution of blasted rock look like? In: Holmberg R (ed) *Proceedings of EFEE 3rd world conference on explosives and blasting*, Brighton, 13–16 September 2005, pp 189–99
- Ouchterlony F (2009a) Fragmentation characterization, the Swebrec function and its use in blast engineering. In: Sanchidrián JA (ed) *Proceedings of 9th international symposium on rock fragmentation by blasting (Fragblast 9)*, Granada, Spain, 13–17 September 2009. CRC Press/Balkema, Leiden, pp 3–22
- Ouchterlony F (2009b) A common form for fragment size distributions from blasting and a derivation of a generalized Kuznetsov's x_{50} -equation. In: Sanchidrián JA (ed) *Proceedings of 9th international symposium on rock fragmentation by blasting (Fragblast 9)*, Granada, Spain, 13–17 September 2009. CRC Press/Balkema, Leiden, pp 199–208
- Ouchterlony F (2016a) The case for the median fragment size as a better fragment size descriptor than the mean. *Rock Mech Rock Eng* 49(1):143–164
- Ouchterlony F (2016b) Reply to discussion of “The case for the median fragment size as a better fragment size descriptor than the mean” by Finn Ouchterlony, *Rock Mech Rock Eng*, published online 15 March 2015. *Rock Mech Rock Eng* 49(1):339–342
- Ouchterlony F, Moser P (2006) Likenesses and differences in the fragmentation of full-scale and model-scale blasts. *Proceedings of 8th international symposium on rock fragmentation by blasting (Fragblast 8)*, Santiago, Chile, 7–11 May 2006. Editec, Santiago, pp 207–220
- Ouchterlony F, Olsson M, Nyberg U, Potts G, Andersson P, Gustavsson L (2005) Optimal fragmentering i krosstäcker—Fältförsök i Vändletäkten. Report 1:11, MinBas Project, Stockholm **(in Swedish)**
- Ouchterlony F, Olsson M, Nyberg U, Andersson P, Gustavsson L (2006) Constructing the fragment size distribution of a bench blasting round, using the new Swebrec function. *Proceedings of 8th international symposium on rock fragmentation by blasting (Fragblast 8)*, Santiago, Chile, 7–11 May 2006. Editec, Santiago, pp 332–344
- Ouchterlony F, Nyberg U, Olsson M, Vikström K, Svedensten P (2010) Optimal fragmentering i krosstäcker, fältförsök i Långåsen. Report 2010:2, MinBas Project 1.2.1: optimal fragmentering vid sprängning II. Swebrec—Swedish Blasting Research Center, Stockholm **(in Swedish)**
- Ouchterlony F, Nyberg U, Olsson M, Widenberg K, Svedensten P (2015) Effects of specific charge and electronic delay detonators on fragmentation in an aggregate quarry, building KCO design curves. In: Spathis AT et al (eds) *Proceedings of 11th international symposium on rock fragmentation by blasting (Fragblast 11)*, Sydney, Australia, 24–26 August 2015. The Australasian Institute of Mining and Metallurgy, Carlton, pp 727–739

- Ouchterlony F, Sanchidrián JA, Moser P (2016) Percentile fragment size predictions for blasted rock and the fragmentation-energy fan. *Rock Mech Rock Eng*. doi:10.1007/s00603-016-1094-x
- Persson PA, Holmberg R, Lee J (1994) *Rock blasting and explosives engineering*. CRC Press, Boca Raton, p 11
- Price D (1981) Detonation reaction zone length and reaction time. In: Zerilli FJ (ed) *Notes on lectures in detonation physics*, Report NSWC MP 81-399. Naval Surface Weapons Center, Dahlgren, VA, pp 191–205
- Raina AK, Ramulu M, Choudhury PB, Dudhankar A, Chakraborty AK (2002) Fragmentation prediction in different rock masses characterised by drilling index. In: Wang XG (ed) *Proceedings of 7th international symposium on rock fragmentation by blasting (Fragblast 7)*, Beijing, 11–15 August 2002. Metallurgical Industry Press, Beijing, pp 117–121
- Raina AK, Ramulu M, Choudhury PB, Chakraborty AK, Sinha A, Ramesh-Kumar B, Fazal M (2009) Productivity improvement in an opencast coal mine in India using digital image analysis technique. In: Sanchidrián JA (ed) *Proceedings of 9th international symposium on rock fragmentation by blasting (Fragblast 9)*, Granada, Spain, 13–17 September 2009. CRC Press/Balkema, Leiden, pp 707–716
- Roberts DK, Wells AA (1954) The velocity of brittle fracture. *Eng Lond* 178:820–821
- Rodger S, Gricius A (2006) Defining the effect of varying fragmentation on overall mine efficiency. *Proceedings of 8th international symposium on rock fragmentation by blasting (Fragblast 8)*, Santiago, Chile, 7–11 May 2006. Editec, Santiago, pp 313–320
- Rollins RR, Wang SW (1990) Fragmentation prediction in bench blasting. *Proceedings of 3rd international symposium on rock fragmentation by blasting*, Brisbane, Australia, 26–31 August 1990. The Australasian Institute of Mining and Metallurgy, Carlton, pp 195–198
- Rosin P, Rammner E (1933) The laws governing the fineness of powdered coal. *J Inst Fuel* 7:29–36
- Rustan A, Nie SL (1987) Fragmentation model at rock blasting. Research report 1987:07. Luleå Tekniska Universitet, Luleå, Sweden
- Sanchidrián JA (2015) Ranges of validity of some distribution functions for blast-fragmented rock. In: Spathis AT et al (eds) *Proceedings of 11th international symposium on rock fragmentation by blasting (Fragblast 11)*, Sydney, Australia, 24–26 August. The Australasian Institute of Mining and Metallurgy, Carlton, pp 741–748
- Sanchidrián JA, Segarra P, López LM (2006) A practical procedure for the measurement of fragmentation by blasting by image analysis. *Rock Mech Rock Eng* 39(4):359–382
- Sanchidrián JA, Castedo R, López LM, Segarra P, Santos AP (2015) Determination of the JWL constants for ANFO and emulsion explosives from cylinder test data. *Central Eur J Energ Mater* 12(2):177–194
- Schimiek P, Ouchterlony F, Moser P (2015) Influence of blasthole delay times on fragmentation as well as characteristics of blast damage behind a remaining bench face through model-scale blasting. In: Spathis AT et al (eds) *Proceedings of 11th international symposium on rock fragmentation by blasting (Fragblast 11)*, Sydney, Australia 24–26 August 2015. The Australasian Institute of Mining and Metallurgy, Carlton, pp 257–265
- Scholz CH (1990) *The mechanics of earthquakes and faulting*. Cambridge University Press, Cambridge, UK, pp 28–29
- Schuhmann R (1940) Principles of comminution, I-size distribution and surface calculations. AIME Technical Pub. no. 1189. American Institute of Mining and Metallurgical Engineers, New York, pp 1–11
- Scott A (1996) ‘Blastability’ and blast design. In: Mohanty B (ed) *Proceedings of 5th international symposium on rock fragmentation by blasting (Fragblast 5)*, Montreal, Canada, 25–29 August 1996. Balkema, Rotterdam, pp 27–36
- Seber GAF, Wild CJ (2003) *Nonlinear regression*. Wiley, Hoboken
- Segarra P, Sanchidrián JA (2003) The effect of blast design parameters on fragmentation in El Alto quarry (Madrid, Spain). Report 92, Less Fines Project, EC Contract no. G1RD-CT-2000-00438. Universidad Politécnica de Madrid
- Sellers E, Kotze M, Mthlane M (2012) Quantification of the effect of inaccurate drilling on the risk of poor fragmentation and increased blast hazard. In: Singh PK, Sinha A (eds) *Proceedings of 10th international symposium on rock fragmentation by blasting (Fragblast 10)*, New Delhi, India, 26–29 November 2012. CRC Press/Balkema, Leiden, pp 153–161
- Singh PK, Roy MP, Drebenstedt C, Prasad B (2015) Blast design parameters and their impact on rock fragmentation. In: Spathis AT et al (eds) *Proceedings of 11th international symposium on rock fragmentation by blasting (Fragblast 11)*, Sydney, Australia, 24–26 August 2015. The Australasian Institute of Mining and Metallurgy, Carlton, pp 755–762
- Smith NS (1976) Burden-rock stiffness and its effects on fragmentation in bench blasting. Ph.D. Thesis, University of Missouri-Rolla
- Spathis AT (2004) A correction relating to the analysis of the original Kuz-Ram model. *Fragblast Int J Blasting Fragn* 8(4):201–205
- Spathis AT (2009) Formulae and techniques for assessing features of blast-induced fragmentation distributions. In: Sanchidrián JA (ed) *Proceedings of 9th international symposium on rock fragmentation by blasting (Fragblast 9)*, Granada, Spain, 13–17 September 2009. CRC Press/Balkema, Leiden, pp 209–219
- Spathis AT (2012) A three parameter rock fragmentation distribution. In: Sanchidrián J, Singh AK (eds) *Measurement and analysis of blast fragmentation*. CRC Press, Taylor & Francis Group, London, pp 73–86
- Spathis AT (2016) Discussion of “The case for the median fragment size as a better fragment size descriptor than the mean” by Finn Ouchterlony, *Rock Mech Rock Eng*, 2015. *Rock Mech Rock Eng* 49(1):335–337
- Stagg MS, Nutting MJ (1987) Influence of blast delay time on rock fragmentation: one-tenth-scale tests. US. Bureau of Mines IC 9135, Minneapolis, MN, USA, pp 79–95
- Stagg MS, Otterness RE (1995) Screen analysis of full-scale production blasts. Proc 11th Symp on Explosives and Blasting Research, Nashville, TN, 5–9 February 1995. International Society of Explosives Engineers, Cleveland, pp 298–313
- Stagg MS, Rholl SA (1987) Effects of accurate delays on fragmentation for single-row blasting in a 6.7 m (22-ft) bench. In: Fourny WL, Dick RD (eds) *Proceedings of 2nd international symposium on rock fragmentation by blasting*, Keystone, CO, 23–26 August 1987. Society of Experimental Mechanics, Bethel, pp 210–223
- Stagg MS, Rholl SA, Otterness RE (1989) The effect of explosive type and delay between rows on fragmentation. *Proceedings of 15th conference on explosives and blasting technique*, New Orleans, LA, 5–10 February 1989. Society of Explosives Engineers, Solon, pp 353–366
- Strelec S, Gazdek M, Mesec J (2011) Blasting design for obtaining desired fragmentation. *Technical Gazette* 18(1):79–86
- Thornton D, Kanchibotla SS, Brunton I (2001) Modelling the impact of rock mass and blast design variation on blast fragmentation. *Proceedings of Explo 2001*, Hunter Valley, NSW, 28–31 October 2001. The Australasian Institute of Mining and Metallurgy, Carlton, pp 197–205
- Tosun A, Konak G, Toprak T, Karakus D, Onur AH (2014) Development of the Kuz-Ram model to blasting in a limestone quarry. *Arch Min Sci* 59(2):477–488

- Vanbrabant F, Espinosa Escobar A (2006) Impact of short delays sequence on fragmentation by means of electronic detonators: theoretical concepts and field validation. Proceedings of 8th international symposium on rock fragmentation by blasting (Fragblast 8), Santiago, Chile, 7–11 May 2006. Editec, Santiago, pp 326–331
- Weibull W (1939) A statistical theory of the strength of materials. *Ingeniörvetenskapsakademiens Handlingar* 151:1–45
- Weibull W (1951) A statistical distribution function of wide applicability. *J Appl Mech Trans ASME* 18:293–297
- Winzer SR, Anderson DA, Ritter AP (1983) Rock fragmentation by explosives. In: Holmberg R, Rustan A (eds) Proceedings of 1st international symposium on rock fragmentation by blasting, Luleå, Sweden, August 23–26. Luleå Tekniska Universitet, Luleå, pp 225–249